

POST-TRAINING QUANTIZATION FOR NEURAL NETWORKS WITH PROVABLE GUARANTEES

JINJIE ZHANG, YIXUAN ZHOU, AND RAYAN SAAB

ABSTRACT. While neural networks have been remarkably successful in a wide array of applications, implementing them in resource-constrained hardware remains an area of intense research. By replacing the weights of a neural network with quantized (e.g., 4-bit, or binary) counterparts, massive savings in computation cost, memory, and power consumption are attained. We modify a post-training neural-network quantization method, GPFQ, that is based on a greedy path-following mechanism, and rigorously analyze its error. We prove that for quantizing a single-layer network, the relative square error essentially decays linearly in the number of weights – i.e., level of over-parametrization. Our result holds across a range of input distributions and for both fully-connected and convolutional architectures. To empirically evaluate the method, we quantize several common architectures with few bits per weight, and test them on ImageNet, showing only minor loss of accuracy. We also demonstrate that standard modifications, such as bias correction and mixed precision quantization, further improve accuracy.

1. INTRODUCTION

Over the past decade, deep neural networks (DNNs) have achieved great success in many challenging tasks, such as computer vision, natural language processing, and autonomous vehicles. Nevertheless, over-parameterized DNNs are computationally expensive to train, memory intensive to store, and energy consuming to apply. This hinders the deployment of DNNs to resource-limited applications. Therefore, model compression without significant performance degradation is an important active area of deep learning research [11, 25, 6, 10]. One prominent approach to compression is *quantization*. Here, rather than adopt a 32-bit floating point format for the model parameters, one uses significantly fewer bits for representing weights, activations, and even gradients. Since the floating-point operations are substituted by more efficient low-bit operations, quantization can reduce inference time and power consumption.

Following [16], we can classify quantization methods into two categories: *quantization-aware training* and *post-training quantization*. The fundamental difficulty in quantization-aware training stems from the fact that it reduces to an integer programming problem with a non-convex loss function, making it NP-hard in general. Nevertheless, many well-performing heuristic methods exist, e.g., [4, 12, 36, 15, 34, 21, 32]. Here one, for example, either modifies the training procedure to produce quantized weights, or successively quantizes each layer and then retrains the subsequent layers. Retraining is a powerful, albeit computationally intensive way to compensate for the accuracy loss resulting from quantization and it remains generally difficult to analyze rigorously.

Hence, much attention has recently been dedicated to post-training quantization schemes, which directly quantize pretrained DNNs, with real-valued weights, without retraining. These quantization methods either rely on a small amount of data [1, 3, 35, 24, 14, 31, 19, 22] or can be implemented without accessing training data, i.e. data-free compression [23, 2, 33, 20]. In this paper, we modify and analyze a robust post-training weight quantization method using a limited amount of training data. We demonstrate that the performance of this quantization method is not only good in experimental settings, but, equally importantly, can be proven to work well with theoretical guarantees.

1.1. Notation. We will use the following notation throughout this paper. Various positive absolute constants are denoted by C, c . We use $a \lesssim b$ as shorthand for $a \leq Cb$, and $a \gtrsim b$ for $a \geq Cb$. Let $S \subseteq \mathbb{R}^n$ be a Borel set. $\text{Unif}(S)$ denotes the uniform distribution over S . A L -layer multi-layer perceptron, Φ , acts on a vector $x \in \mathbb{R}^{N_0}$ via

$$(1) \quad \Phi(x) := \varphi^{(L)} \circ A^{(L)} \circ \dots \circ \varphi^{(1)} \circ A^{(1)}(x)$$

where $\varphi^{(i)} : \mathbb{R}^{N_i} \rightarrow \mathbb{R}^{N_i}$ is an activation function acting entrywise, and $A^{(i)} : \mathbb{R}^{N_{i-1}} \rightarrow \mathbb{R}^{N_i}$ is an affine map given by $A^{(i)}(z) := W^{(i)\top}z + b^{(i)}$. Here, $W^{(i)} \in \mathbb{R}^{N_{i-1} \times N_i}$ is a weight matrix and $b^{(i)} \in \mathbb{R}^{N_i}$ is a bias vector. Since $w^\top x + b = \langle (w, b), (x, 1) \rangle$, the bias term $b^{(i)}$ can simply be treated as an extra row to the weight matrix $W^{(i)}$, so we will henceforth ignore it. We focus on *midrise* alphabets

$$(2) \quad \mathcal{A} = \mathcal{A}_K^\delta := \{\pm(k - 1/2)\delta : 1 \leq k \leq K, k \in \mathbb{Z}\}$$

and *midtreed* alphabets

$$(3) \quad \mathcal{A} = \widetilde{\mathcal{A}}_K^\delta := \{\pm k\delta : 0 \leq k \leq K, k \in \mathbb{Z}\}$$

where $\delta > 0$ denotes the quantization step size. For example, $\mathcal{A}_1^2 = \{\pm 1\}$ is a 1-bit alphabet while $\widetilde{\mathcal{A}}_1^1 = \{0, \pm 1\}$ is a ternary alphabet. Moreover, the following augmented midrise alphabets can also be used in practice:

$$(4) \quad \hat{\mathcal{A}}_K^\delta := \mathcal{A}_K^\delta \cup \{0\}.$$

For any alphabet, we define the associated *memoryless scalar quantizer* (MSQ) $\mathcal{Q} : \mathbb{R} \rightarrow \mathcal{A}$ by

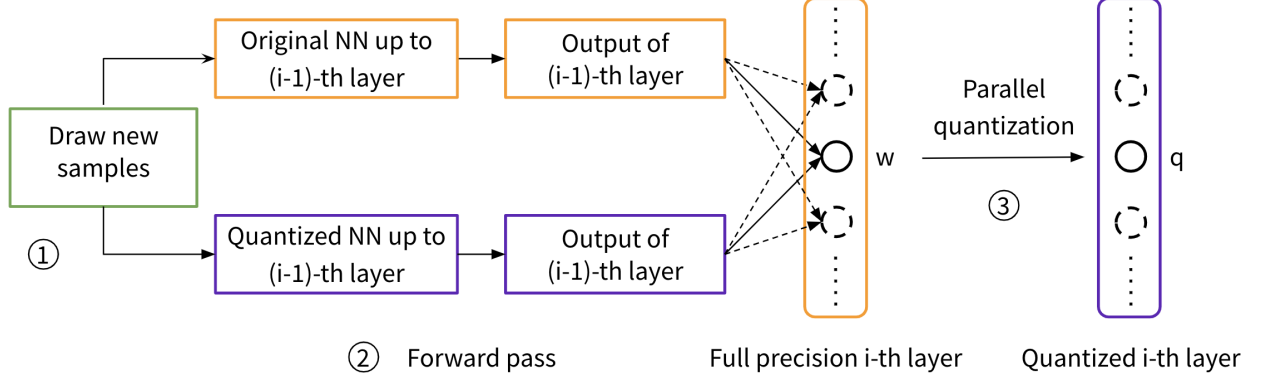
$$(5) \quad \mathcal{Q}(z) := \operatorname{argmin}_{p \in \mathcal{A}} |z - p|.$$

1.2. Related Work. Now we summarize some prior work on post-training quantization methods. We note that the majority of them aims to reduce quantization error by minimizing a mean squared error (MSE) objective, e.g.

$$\min_{\alpha > 0} \left\| W - \alpha \left\lfloor \frac{W}{\alpha} \right\rfloor \right\|_F$$

where W is a weight matrix and $\lfloor \cdot \rfloor$ is a round-off operator. In such methods, once the quantization bins are selected, weights are quantized independently of each other. Nevertheless, these works use different strategies for determining the quantization bins. For example, Banner et al. [1] (see also [35]) choose the thresholds to minimize a MSE metric. Their numerical results also show that for convolutional networks using different quantization thresholds “per-channel” and bias correction can improve the accuracy of quantized models. Choukroun et al. [3] solve a minimum mean squared error (MMSE) problem for both weights and activations quantization. Based on a small calibration data set, Hubara et al. [14] suggest a per-layer optimization method followed by integer programming to determine the bit-width of different layers. A bit-split and stitching technique is used by [31] that “splits” integers into multiple bits, then optimizes each bit, and finally stitches all bits back to integers. Li et al. [19] leverage the basic building blocks in DNNs and reconstructs them one-by-one. As for data-free model quantization, there are different strategies, such as weight equalization [23], reconstructing calibration data samples according to batch normalization statistics (BNS) [2, 33], and adversarial learning [20].

1.3. GPFQ and Contributions. In spite of convincing heuristic explanations and reasonable empirical results, all quantization methods mentioned in Section 1.2 lack rigorous theoretical guarantees. Recently, Lybrand and Saab [22] proposed, and analyzed, a method for quantizing the weights of pretrained DNNs, namely *greedy path following quantization* (GPFQ). Specifically, given a data set $X \in \mathbb{R}^{m \times N_0}$ with vectorized data stored as rows and a trained neural network Φ with weight matrices $W^{(i)}$, the GPFQ algorithm is a map $W^{(i)} \rightarrow Q^{(i)} \in \mathcal{A}^{N_{i-1} \times N_i}$, giving a new quantized neural network $\tilde{\Phi}$ with $\tilde{\Phi}(X) \approx \Phi(X)$. The matrices $W^{(1)}, \dots, W^{(L)}$ are quantized


 FIGURE 1. GPFQ: Quantize the i -th layer of a neural network.

sequentially and in each layer every neuron (a column of $W^{(i)}$) is quantized independently of other neurons, which allows parallel quantization across neurons in a layer.

Thus, GPFQ can be implemented recursively as illustrated in Figure 1. Let $\Phi^{(i)}$, $\tilde{\Phi}^{(i)}$ denote the original and quantized neural networks up to layer i respectively. Assume the first $i - 1$ layers have been quantized and define $X^{(i-1)} := \Phi^{(i-1)}(X)$, $\tilde{X}^{(i-1)} := \tilde{\Phi}^{(i-1)}(X) \in \mathbb{R}^{m \times N_{i-1}}$. Then each neuron $w \in \mathbb{R}^{N_{i-1}}$ in layer i is quantized by constructing $q \in \mathcal{A}^{N_{i-1}}$ such that

$$\tilde{X}^{(i-1)} q = \sum_{t=1}^{N_{i-1}} q_t \tilde{X}_t^{(i-1)} \approx \sum_{t=1}^{N_{i-1}} w_t X_t^{(i-1)} = X^{(i-1)} w$$

where $X_t^{(i-1)}$, $\tilde{X}_t^{(i-1)}$ are the t -th columns of $X^{(i-1)}$, $\tilde{X}^{(i-1)}$. This is done by selecting q_t , for $t = 1, 2, \dots, N_{i-1}$, so the running sum $\sum_{j=1}^t q_j \tilde{X}_j^{(i-1)}$ tracks its analog $\sum_{j=1}^t w_j X_j^{(i-1)}$ as well as possible in an ℓ_2 sense. So,

$$(6) \quad q_t = \arg \min_{p \in \mathcal{A}} \left\| \sum_{j=1}^t w_j X_j^{(i-1)} - \sum_{j=1}^t p_j \tilde{X}_j^{(i-1)} - p \tilde{X}_t^{(i-1)} \right\|_2^2.$$

This is equivalent to the following iteration, which facilitates the analysis of the approximation error:

$$(7) \quad \begin{cases} u_0 = 0 \in \mathbb{R}^m, \\ q_t = \arg \min_{p \in \mathcal{A}} \|u_{t-1} + w_t X_t^{(i-1)} - p \tilde{X}_t^{(i-1)}\|_2^2, \\ u_t = u_{t-1} + w_t X_t^{(i-1)} - q_t \tilde{X}_t^{(i-1)}. \end{cases}$$

By induction, one can verify that $u_t = \sum_{j=1}^t (w_j X_j^{(i-1)} - q_j \tilde{X}_j^{(i-1)})$ for $t = 0, 1, \dots, N_{i-1}$, and thus $\|u_{N_{i-1}}\|_2 = \|X^{(i-1)} w - \tilde{X}^{(i-1)} q\|_2$. Moreover, one can derive a closed-form expression of q_t in (7) as

$$(8) \quad q_t = \mathcal{Q} \left(\frac{\langle \tilde{X}_t^{(i-1)}, u_{t-1} + w_t X_t^{(i-1)} \rangle}{\|\tilde{X}_t^{(i-1)}\|_2^2} \right),$$

which is proved in Lemma A.1. The whole algorithm for quantizing multilayer perceptrons (MLPs) is summarized in Algorithm 1. For the i -th layer, this parallelizable algorithm has run time complexity $O(mN_{i-1})$. Note that in order to quantize convolutional neural networks (CNNs), one can simply vectorize the sliding (convolutional) kernels and unfold, i.e., vectorize, the corresponding image patches. Then, taking the usual inner product on vectors, one can reduce to the case of MLPs, also see Section 2.3.

Our specific contributions are threefold:

Algorithm 1: Using GPFQ to quantize MLPs

Input: A L -layer MLP Φ with weight matrices $W^{(i)} \in \mathbb{R}^{N_{i-1} \times N_i}$, input mini-batches $\{X_i\}_{i=1}^L \subset \mathbb{R}^{m \times N_0}$

```

1 for  $i = 1$  to  $L$  do
2   Phase I: Forward propagation
3   Generate  $X^{(i-1)} = \Phi^{(i-1)}(X_i) \in \mathbb{R}^{m \times N_{i-1}}$ 
4   Generate  $\tilde{X}^{(i-1)} = \tilde{\Phi}^{(i-1)}(X_i) \in \mathbb{R}^{m \times N_{i-1}}$ 
5   Phase II: Parallel quantization for  $W^{(i)}$ 
6   repeat
7     Pick a column (neuron)  $w \in \mathbb{R}^{N_{i-1}}$  of  $W^{(i)}$ 
8     for  $t = 1$  to  $N_{i-1}$  do
9        $u_0 = 0 \in \mathbb{R}^m$ 
10       $q_t = \mathcal{Q}\left(\frac{\langle \tilde{X}_t^{(i-1)}, u_{t-1} + w_t X_t^{(i-1)} \rangle}{\|\tilde{X}_t^{(i-1)}\|_2^2}\right)$ 
11       $u_t = u_{t-1} + w_t X_t^{(i-1)} - q_t \tilde{X}_t^{(i-1)}$ 
12    until All columns of  $W^{(i)}$  are quantized
13  Obtain quantized  $i$ -th layer  $Q^{(i)} \in \mathcal{A}^{N_{i-1} \times N_i}$ 

```

Output: Quantized neural network $\tilde{\Phi}$

- We generalize the results of [22] in several directions. The results of [22] apply only to a ternary GPFQ with standard Gaussian input, under the assumption that floating point weights are ϵ -away from alphabet elements. By contrast, our results avoid this assumption and extend to general alphabets like (2) and (3). Meanwhile, the main result in [22] becomes a special case of our Theorem 2.2. Moreover, we extend the class of input vectors for which the theory applies. For example, in Section 2, we show that if the input data $X \in \mathbb{R}^{m \times N_0}$ is either bounded or drawn from a mixture of Gaussians, then the relative square error of quantizing a neuron $w \in \mathbb{R}^{N_0}$ satisfies the following inequality with high probability:

$$\frac{\|Xw - Xq\|_2^2}{\|Xw\|_2^2} \lesssim \frac{m\delta^2 \log N_0}{N_0}$$

where $\delta > 0$ is the step size in (2) and (3). Additionally, similar error bounds of quantizing single-layer CNNs are derived for the first time.

- With regards to CNNs, fixing kernel size and padding in a convolutional layer, the number of local blocks, i.e. image patches, obtained from each image is $T := O(HW/(S_H S_W))$ where (H, W) and (S_H, S_W) are image size and stride respectively. For large input images with small stride, the computational complexity of quantizing CNNs in [22] blows up because one has to implement (7) with $m = BT$. Here, B denotes batch size. This explains why Lybrand and Saab [22] only quantized the fully connected layers of VGG-16 in their numerical experiments. To overcome this issue, we modify GPFQ by extracting sliding blocks (used for quantization) with the stride being equal to kernel size and introducing a sampling probability $p \in (0, 1)$. That is, we randomly select a proportion p of the vectorized disjoint image patches; see Section 3.1. These particular modifications also enable the theoretical guarantees on CNN quantization that we obtain in Section 2.3.
- In our experiments in Section 3, we compare our method with other post-training quantization approaches and show that it achieves near-original model performance using 4 bits and that the results for 5 bits are competitive with state-of-the-art methods across common computer vision architectures. Moreover, since GPFQ is a per-layer quantization method

with uniform alphabet and fixed bit-width for all layers, it is efficient and flexible in the sense that GPFQ reduces the complexity for inference architecture design and is compatible with various tricks such as bias correction [1], unquantizing the last layer [36, 19], and mixed precision [7, 2]. Hence, the performance of GPFQ can be further improved by incorporating these techniques.

2. NEW THEORETICAL RESULTS

In this section, we will present error bounds for GPFQ with single-layer networks Φ in (1) with $L = 1$. So we quantize the weight matrix $W := W^{(1)} \in \mathbb{R}^{N_0 \times N_1}$ and implement (7) and (8) using $i = 1$. Defining the input data $X := X^{(0)} = \widetilde{X}^{(0)} \in \mathbb{R}^{m \times N_0}$, the iteration can be expressed as

$$(9) \quad \begin{cases} u_0 = 0 \in \mathbb{R}^m, \\ q_t = \mathcal{Q}\left(w_t + \frac{X_t^\top u_{t-1}}{\|X_t\|_2}\right), \\ u_t = u_{t-1} + w_t X_t - q_t X_t. \end{cases}$$

Moreover, we have $u_t = \sum_{j=1}^t (w_j X_j - q_j X_j)$ for $t = 1, 2, \dots, N_0$. Clearly, our goal is to control $\|u_t\|_2$. In particular, given $t = N_0$, we recover the ℓ_2 distance between full-precision and quantized pre-activations: $\|u_{N_0}\|_2 = \|Xw - Xq\|_2$.

2.1. Bounded Input Data. We start with a quantization error bound proved in Appendix B, where the feature vectors, i.e. columns, of the input data matrix $X \in \mathbb{R}^{m \times N_0}$ are bounded. This general result is then applied to data drawn uniformly from a Euclidean ball, and to Bernoulli random data, showing that the resulting relative square error due to quantization decays linearly with the width N_0 of the network.

Theorem 2.1 (Bounded input data). *Suppose that the columns X_t of $X \in \mathbb{R}^{m \times N_0}$ are drawn independently from a probability distribution for which there exists $s \in (0, 1)$ and $r > 0$ such that $\|X_t\|_2 \leq r$ almost surely, and such that for all unit vector $u \in \mathbb{S}^{m-1}$ we have*

$$(10) \quad \mathbb{E} \frac{\langle X_t, u \rangle^2}{\|X_t\|_2^2} \geq s^2.$$

Let \mathcal{A} be the alphabet in (2) or (3) with step size $\delta > 0$, and largest element q_{\max} . Let $w \in \mathbb{R}^{N_0}$ be the weights associated with a neuron, with $\|w\|_\infty \leq q_{\max}$. Quantizing w using (9), we have

$$\mathbb{P}\left(\|Xw - Xq\|_2^2 \leq \frac{r^2 \delta^2}{s^2} \log N_0\right) \geq 1 - \frac{1}{N_0^2} \left(2 + \frac{1}{\sqrt{1-s^2}}\right),$$

and

$$\mathbb{P}\left(\max_{1 \leq t \leq N_0} \|u_t\|_2^2 \leq \frac{r^2 \delta^2}{s^2} \log N_0\right) \geq 1 - \frac{1}{N_0} \left(2 + \frac{1}{\sqrt{1-s^2}}\right).$$

Furthermore, if the activation function $\varphi : \mathbb{R} \rightarrow \mathbb{R}$ is L -Lipschitz continuous, that is, $|\varphi(x) - \varphi(y)| \leq L|x - y|$ for all $x, y \in \mathbb{R}$, then we have

$$\mathbb{P}\left(\|\varphi(Xw) - \varphi(Xq)\|_2^2 \leq \frac{r^2 \delta^2 L^2}{s^2} \log N_0\right) \geq 1 - \frac{1}{N_0^2} \left(2 + \frac{1}{\sqrt{1-s^2}}\right).$$

Next, we apply Theorem 2.1 to uniformly distributed and Bernoulli distributed input data X .

Uniform Distribution. Let $B_r \subset \mathbb{R}^m$ be the closed ball with center 0 and radius $r > 0$. Suppose that columns X_t of $X \in \mathbb{R}^{m \times N_0}$ are drawn i.i.d. from $\text{Unif}(B_r)$. Then $\|X_t\|_2 \leq r$ and $Z := X_t / \|X_t\|_2 \sim \text{Unif}(\mathbb{S}^{m-1})$. Since Z is rotation invariant, for any unit vector $u \in \mathbb{S}^{m-1}$, we have

$$\mathbb{E} \left\langle \frac{X_t}{\|X_t\|_2}, u \right\rangle^2 = \mathbb{E} \langle Z, u \rangle^2 = \mathbb{E} \langle Z, e_1 \rangle^2 = \mathbb{E} Z_1^2 = \frac{1}{m}.$$

The last equality holds because $\|Z\|_2 = 1$ and $\mathbb{E}Z_1^2 = \mathbb{E}Z_2^2 = \dots = \mathbb{E}Z_m^2 = \frac{1}{m}\mathbb{E}\left(\sum_{i=1}^m Z_i^2\right) = \frac{1}{m}$. So Theorem 2.1 implies that, with high probability

$$(11) \quad \|Xw - Xq\|_2^2 \leq mr^2\delta^2 \log N_0.$$

Moreover, by Lemma A.2, $\mathbb{E}\|X_t\|_2^2 = \frac{mr^2}{m+2}$. It follows that $\mathbb{E}(X^\top X) = \mathbb{E}\|X_1\|_2^2 I_{N_0} = \frac{mr^2}{m+2} I_{N_0}$ and thus

$$\mathbb{E}\|Xw\|_2^2 = w^\top \mathbb{E}(X^\top X)w = \frac{mr^2}{m+2} \|w\|_2^2.$$

If the weight vector $w \in \mathbb{R}^{N_0}$ is *generic* in the sense that $\|w\|_2^2 \gtrsim N_0$, then

$$(12) \quad \mathbb{E}\|Xw\|_2^2 \gtrsim \frac{mN_0r^2}{m+2}.$$

Combining (11) with (12), the relative error can be approximated by

$$\frac{\|Xw - Xq\|_2^2}{\|Xw\|_2^2} \lesssim \frac{m\delta^2 \log N_0}{N_0}.$$

Symmetric Bernoulli Distribution. We say that a random vector $Z = (Z_1, Z_2, \dots, Z_m)$ is *symmetric Bernoulli* if the coordinates Z_i are independent and $\mathbb{P}(Z_i = 1) = \mathbb{P}(Z_i = -1) = \frac{1}{2}$. Now assume that columns X_t of $X \in \mathbb{R}^{m \times N_0}$ are independent and subject to symmetric Bernoulli distribution. Clearly, $\|X_t\|_2 = \sqrt{m}$. If $u \in \mathbb{R}^m$ is a unit vector, then

$$\mathbb{E} \frac{\langle X_t, u \rangle^2}{\|X_t\|_2^2} = \frac{u^\top \mathbb{E}(X_t X_t^\top) u}{m} = \frac{\|u\|_2^2}{m} = \frac{1}{m}.$$

Hence, by Theorem 2.1,

$$(13) \quad \|Xw - Xq\|_2^2 \leq m^2\delta^2 \log N_0$$

holds with high probability. Again, a generic $w \in \mathbb{R}^{N_0}$ with $\|w\|_2^2 \gtrsim N_0$ satisfies

$$\mathbb{E}\|Xw\|_2^2 = w^\top \mathbb{E}(X^\top X)w = m\|w\|_2^2 \gtrsim mN_0$$

and therefore

$$\frac{\|Xw - Xq\|_2^2}{\|Xw\|_2^2} \lesssim \frac{m\delta^2 \log N_0}{N_0}.$$

2.2. Gaussian Clusters. Here, we consider data drawn from Gaussian clusters, which unlike the previously considered models, are unbounded. Specifically, suppose our samples are drawn from d normally distributed clusters $\mathcal{K}_i := \mathcal{N}(z^{(i)}, \sigma^2 I_{N_0})$ with fixed centers $z^{(i)} \in \mathbb{R}^{N_0}$ and $\sigma > 0$. Suppose, for simplicity, that we independently draw n samples from each cluster and vertically stack them in order as rows of X (this ordering does not affect our results in Theorem 2.2). Let $m := nd$. So, for $1 \leq i \leq d$, the row indices of X ranging from $(i-1)n+1$ to in come from cluster \mathcal{K}_i . Then the t -th column of X is of the form

$$(14) \quad X_t = [Y_t^{(1)}, Y_t^{(2)}, \dots, Y_t^{(d)}]^\top \in \mathbb{R}^m$$

where $Y_t^{(i)} \sim \mathcal{N}(z_t^{(i)} \mathbb{1}_n, \sigma^2 I_n)$.

Theorem 2.2 (Gaussian clusters). *Let $X \in \mathbb{R}^{m \times N_0}$ be as in (14) and let \mathcal{A} be as in (2) or (3), with step size $\delta > 0$ and largest element q_{\max} . Let $p \in \mathbb{N}$, $K := 1 + \sigma^{-2} \max_{1 \leq i \leq d} \|z^{(i)}\|_\infty^2$, and $w \in \mathbb{R}^{N_0}$ be the weights associated with a neuron, with $\|w\|_\infty \leq q_{\max}$. Quantizing w using (9), we have*

$$\mathbb{P}\left(\|Xw - Xq\|_2^2 \geq 4pm^2 K^2 \delta^2 \sigma^2 \log N_0\right) \lesssim \frac{\sqrt{mK}}{N_0^p}.$$

and

$$P\left(\max_{1 \leq t \leq N_0} \|u_t\|_2^2 \geq 4pm^2K^2\delta^2\sigma^2 \log N_0\right) \lesssim \frac{\sqrt{mK}}{N_0^{p-1}}.$$

If the activation function φ is L -Lipschitz continuous, then

$$P\left(\|\varphi(Xw) - \varphi(Xq)\|_2^2 \geq 4pm^2K^2L^2\delta^2\sigma^2 \log N_0\right) \lesssim \frac{\sqrt{mK}}{N_0^p}.$$

The proof of Theorem 2.2 can be found in Appendix C.

Normal Distribution. As a special case of (14), $X \in \mathbb{R}^{m \times N_0}$ is a Gaussian matrix with $X_{ij} \stackrel{i.i.d.}{\sim} \mathcal{N}(0, \sigma^2)$ when $d = 1$, $n = m$, and $z^{(1)} = 0$. Theorem 2.2 implies that $K = 1$ and

$$(15) \quad P\left(\|Xw - Xq\|_2^2 \geq 4pm^2\delta^2\sigma^2 \log N_0\right) \lesssim \frac{\sqrt{m}}{N_0^p}.$$

Further, suppose that $w \in \mathbb{R}^{N_0}$ is generic, i.e. $\|w\|_2^2 \gtrsim N_0$. In this case, $\mathbb{E}\|Xw\|_2^2 = m\sigma^2\|w\|_2^2 \gtrsim m\sigma^2N_0$. So, with high probability, the relative error in our quantization satisfies

$$(16) \quad \frac{\|Xw - Xq\|_2^2}{\|Xw\|_2^2} \lesssim \frac{m\delta^2 \log N_0}{N_0}.$$

Thus, here again, the relative square error for quantizing a single-layer MLP decays linearly (up to a log factor) in the number of neurons N_0 . Note that (16), for ternary alphabets, is the main result given by [22], which we now obtain as a special case of Theorem 2.2.

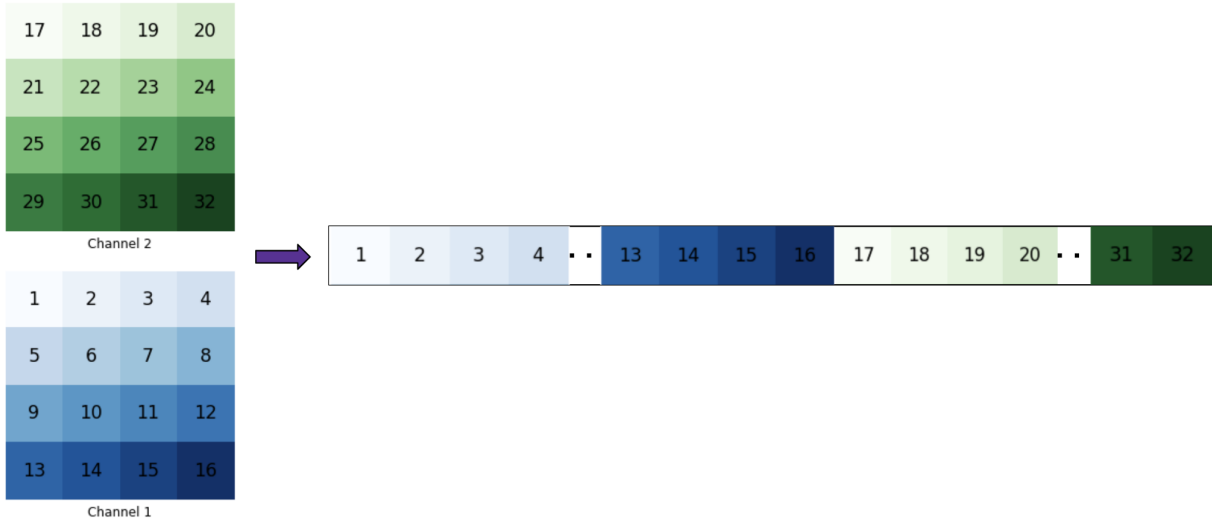


FIGURE 2. Illustration of vectorizing local blocks and kernels when $C_{in} = 2$ and $k_1 = k_2 = 4$.

2.3. Convolutional Neural Networks. In this section, we derive error bounds for single-layer CNNs. Let $Z \in \mathbb{R}^{B \times C_{in} \times S_1 \times S_2}$ be a mini-batch of images with batch size B , input channels C_{in} , height S_1 , and width S_2 . Suppose that all entries of Z are i.i.d. drawn from $\mathcal{N}(0, 1)$ and suppose we have C_{out} convolutional kernels $\{w_i\}_{i=1}^{C_{out}} \subseteq \mathbb{R}^{C_{in} \times k_1 \times k_2}$. Let these kernels “slide” over Z with fixed stride (k_1, k_2) such that sliding local blocks generated by moving w_i on Z are disjoint. Additionally, if T is the number of randomly selected sliding local blocks (in $\mathbb{R}^{C_{in} \times k_1 \times k_2}$) from each image, then one can vectorize all BT local blocks, see Figure 2, and stack them together to obtain a single data

matrix $X \in \mathbb{R}^{BT \times C_{\text{in}} k_1 k_2}$. Moreover, each kernel w_i can be viewed as a column vector in $\mathbb{R}^{C_{\text{in}} k_1 k_2}$ and thus $W = [w_1, w_2, \dots, w_{C_{\text{out}}}] \in \mathbb{R}^{C_{\text{in}} k_1 k_2 \times C_{\text{out}}}$ is the weight matrix to be quantized.

We need to convert W to $Q = [q_1, q_2, \dots, q_{C_{\text{out}}}] \in \mathcal{A}^{C_{\text{in}} k_1 k_2 \times C_{\text{out}}}$ in the spirit of $XQ \approx XW$. Since extracted local blocks from Z are disjoint, columns of X are independent and subject to $\mathcal{N}(0, I_{BT})$. Hence, one can apply (15) with $m = BT$, $N_0 = C_{\text{in}} k_1 k_2$, $\sigma = 1$, and any $p \in \mathbb{N}$. Specifically, for $1 \leq i \leq C_{\text{out}}$, we get

$$\mathbb{P}\left(\|Xw_i - Xq_i\|_2^2 \geq 4pB^2T^2\delta^2 \log(C_{\text{in}} k_1 k_2)\right) \lesssim \frac{\sqrt{BT}}{(C_{\text{in}} k_1 k_2)^p}.$$

By a union bound,

$$\mathbb{P}\left(\max_{1 \leq i \leq C_{\text{out}}} \|Xw_i - Xq_i\|_2^2 \geq 4pB^2T^2\delta^2 \log(C_{\text{in}} k_1 k_2)\right) \lesssim \frac{C_{\text{out}}\sqrt{BT}}{(C_{\text{in}} k_1 k_2)^p}.$$

3. EXPERIMENTS

To evaluate the performance of our method and compare it with the approaches reviewed in Section 1.2, we test our modified GPFQ on the ImageNet classification task¹. In particular, we focus on ILSVRC-2012 [5], a 1000-category dataset with over 1.2 million training images and 50 thousand validation images. All images in ILSVRC-2012 are preprocessed in a standard manner before they are fed into neural networks: we resize each image to 256×256 and use the normalized 224×224 center crop. The evaluation metrics we use are top-1 and top-5 accuracy of the quantized models on the validation dataset.

3.1. Experimental Setup. For reproducibility and fairness of comparison, we use the pretrained 32-bit floating point neural networks provided by torchvision² in PyTorch [26]. We test several well-known neural network architectures including: AlexNet [17], VGG-16 [27], GoogLeNet [28], ResNet-18, ResNet-50 [13], and EfficientNet-B1 [29].

Let $b \in \mathbb{N}$ denote the number of bits used for quantization. Here, we fix b for all the layers. Then, in our experiment, we adopt the augmented midrise alphabets $\hat{\mathcal{A}}_K^\delta$ in (4) with

$$(17) \quad K = 2^{b-1}, \quad \delta = \frac{2R}{2^b - 1},$$

where $R > 0$ is a hyper-parameter. Indeed, according to (2) and (4), $\hat{\mathcal{A}}_K^\delta$ is symmetric with maximal element $q_{\max} = (K - \frac{1}{2})\delta = R$. Since b is fixed, all that remains is to select R in (17) based on the distribution of weights. To that end, suppose we are quantizing the i -th layer of a neural network with weight matrix $W^{(i)} \in \mathbb{R}^{N_{i-1} \times N_i}$. Then, Theorem 2.1 and Theorem 2.2 require that $R = q_{\max} \geq \max_{k,j} |W_{k,j}^{(i)}|$, and yield error bounds that favor a smaller step size $\delta \propto R$. In practice, however, the weights may have outliers with large magnitudes, which would entail unnecessarily using a large R . Thus, rather than choosing $R = \max_{k,j} |W_{k,j}^{(i)}|$, we will consider the average infinity norm of weights across all neurons w , i.e. columns of $W^{(i)}$. That is

$$(18) \quad R \propto \frac{1}{N_i} \sum_{1 \leq j \leq N_i} \|W_j^{(i)}\|_\infty.$$

Combining (18) with (17), the step size used for quantizing the i -th layer is given by

$$(19) \quad \delta^{(i)} := \frac{2C}{(2^b - 1)N_i} \sum_{1 \leq j \leq N_i} \|W_j^{(i)}\|_\infty.$$

¹Our code for experiments is available: https://github.com/YixuanSeanZhou/Quantized_Neural_Nets.git

²<https://pytorch.org/vision/stable/models.html>

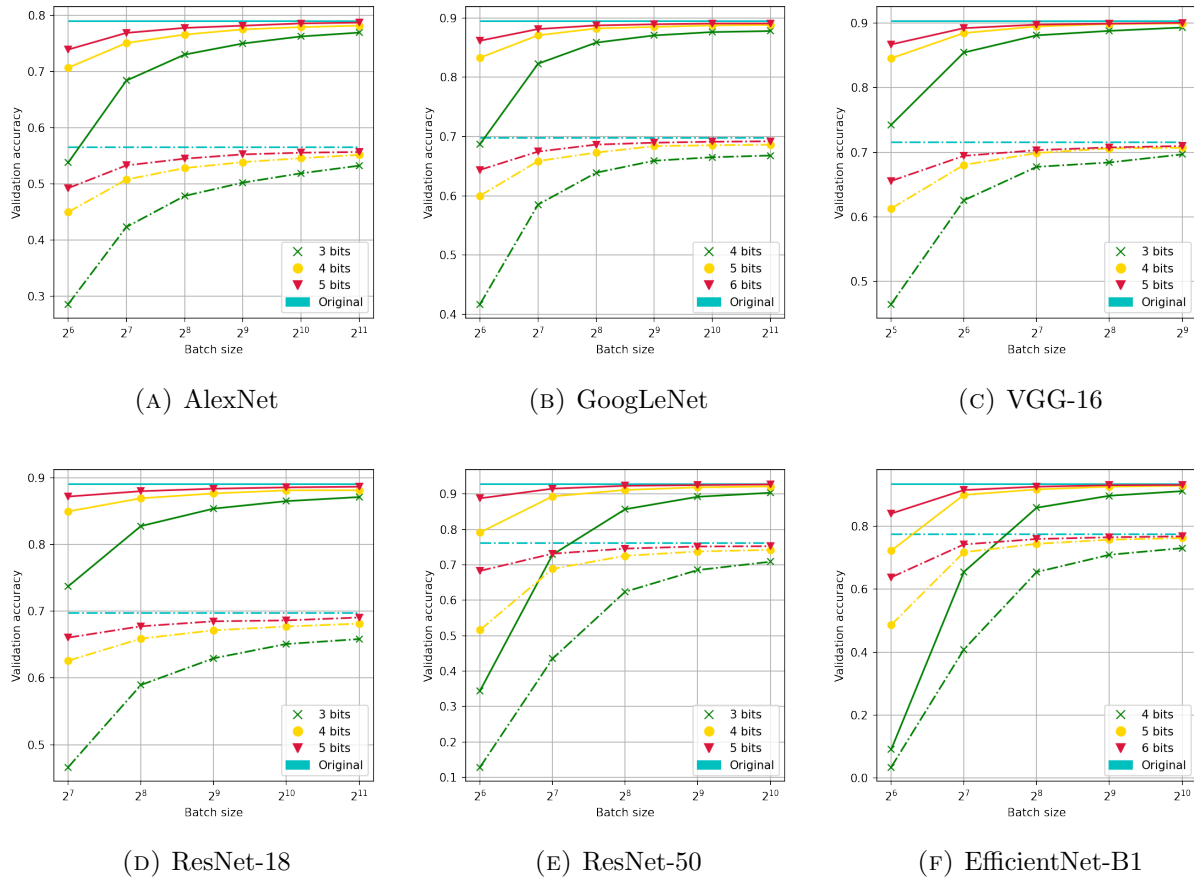


FIGURE 3. Top-1 (dashed line) and Top-5 (solid line) accuracy for original and quantized models on ImageNet.

Here, $C > 0$ is independent of i , determined by grid search with cross-validation, and fixed across layers, and across batch-sizes and bit widths. We comment that a more thorough search for an optimal C depending on these individual parameters may improve performance.

As mentioned in Section 2.3, we introduce a sampling probability $p \in (0, 1]$, associated with GPFQ for convolutional layers. This is motivated, in part, by decreasing the computational cost associated with quantizing such layers. Indeed, a batched input tensor of a convolutional layer can be unfolded as a stack of vectorized sliding local blocks, i.e., a matrix. Since, additionally, the kernel can be reshaped into a column vector, matrix-vector multiplication followed by reshaping gives the output of this convolutional layer. On the other hand, due to potentially large overlaps between sliding blocks, the associated matrices have large row size and thus the computational complexity is high. To accelerate our computations, we extract the data used for quantization by setting the stride (which defines the step size of the kernel when sliding through the image) equal to the kernel size and choosing $p = 0.25$. This choice gives a good trade-off between accuracy and computational complexity, which both increase with p . Recall that the batch size $m \in \mathbb{N}$ denotes the number of samples used for quantizing each layer of a neural network. In all experiments, b is chosen from $\{3, 4, 5, 6\}$.

3.2. Results on ImageNet.

TABLE 1. Top-1/Top-5 accuracy drop using $b = 5$ bits.

Model	C	m	Acc Drop (%)
AlexNet	1.1	2048	0.85/0.33
GoogLeNet	1.41	2048	0.60/0.46
VGG-16	0.975	512	0.63/ 0.32
ResNet-18	1.16	2048	0.71/ 0.44
ResNet-50	1.81	1024	0.90/ 0.19
EfficientNet-B1	1.6	1024	0.76/ 0.40

3.2.1. Impact of b and m . The first experiment is designed to explore the effect of the batch size m , as well as bit-width b , on the accuracy of the quantized models. We compute the validation accuracy of quantized networks with respect to different choices of b and m . In particular, Table 1 shows that, using $b = 5$ bits, all quantized models achieve less than 1% loss in top-1 and top-5 accuracy. Moreover, we illustrate the relationship between the quantization accuracy and the batch size m in Figure 3, where the horizontal lines in cyan, obtained directly from the original validation accuracy of unquantized models, are used for comparison against our quantization method. We observe that (1) all curves with distinct b quickly approach an accuracy ceiling while curves with high b eventually reach a higher ceiling; (2) Quantization with $b \geq 4$ attains near-original model performance if m is sufficiently large; (3) one can expect to obtain higher quantization accuracy by taking larger m but the extra improvement that results from increasing the batch size rapidly diminishes.

3.2.2. Comparisons with Baselines. Next, we compare GPFQ against other post-training quantization schemes discussed in Section 1.2 on various architectures. We note, however, that for a fixed architecture each post-training quantization method starts with a potentially different set of parameters (weights and biases), and these parameters are not available to us. As such, we simply report other methods’ accuracies as they appear in their associated papers. Due to this, a perfect comparison between methods is not possible. Another factor that impacts the comparison is that following DoReFa-Net [37], many baseline quantization schemes [35, 14, 19] leave the first and the last layers of DNNs unquantized to alleviate accuracy degradation. On the other hand, we quantize *all* layers of the model. Table 2 displays the number of bits and the method used to quantize each network. It also contains the accuracy of quantized and full-precision models respectively, as well as their difference, i.e. accuracy drop. We report the results of GPFQ for all models with $b = 3, 4, 5$. The important observation here is that our method is competitive across architectures and bit-widths, and shows the best performance on a number of them.

3.2.3. Further Improvement of GPFQ. For our final experiment, we show that the validation accuracy of the proposed approach can be further improved by incorporating the following modifications used by prior work: (1) mixing precision for quantization, such as using different bit-widths to quantize fully-connected and convolutional layers respectively [2] or leaving the last fully-connected layer unquantized [37]; (2) applying bias correction [1, 23] to the last layer, that is, subtracting the average quantization error from the layer’s bias term. In Table 3, we examine some of these empirical rules by leaving the last layer intact and performing bias correction to remove the noise due to quantization. This variant of GPFQ is highlighted by a † symbol. Table 3 also presents a more comprehensive comparisons of our results with other methods. By using the enhanced GPFQ, the average increment of accuracy exceeds 0.2% for $b = 4, 5$ bits, and is greater than 0.7% for $b = 3$ bits. This demonstrates, empirically, that GPFQ can be easily adapted to incorporate heuristic modifications that improve performance.

TABLE 2. ImageNet Top-1 accuracy with weight quantization.

Model	Bits	Method	Quant Acc (%)	Ref Acc (%)	Acc Drop (%)
Alexnet	3	GPFQ (Ours)	53.22	56.52	3.30
	4	OMSE[3]	55.52	56.62	1.10
		GPFQ (Ours)	55.15	56.52	1.37
	5	GPFQ (Ours)	55.67	56.52	0.85
	8	DoReFa [37]	53.00	55.90	2.90
VGG-16	3	GPFQ (Ours)	69.67	71.59	1.92
	4	MSE [1]	70.50	71.60	1.10
		OMSE [3]	71.48	73.48	2.00
		GPFQ (Ours)	70.70	71.59	0.89
	5	GPFQ (Ours)	70.96	71.59	0.63
8	Lee et al. [18]	68.05	68.34	0.29	
ResNet-18	3	GPFQ (Ours)	65.81	69.75	3.94
	4	MSE [1]	67.00	69.70	2.70
		OMSE [3]	68.38	69.64	1.26
		S-AdaQuant [14]	69.40	71.97	2.57
		AdaRound [24]	68.71	69.68	0.97
		BRECQ [19]	70.70	71.08	0.38
		GPFQ (Ours)	68.13	69.76	1.63
	5	RQ [21]	65.10	69.54	4.44
		GPFQ (Ours)	69.04	69.75	0.71
	6	DFQ [23]	66.30	70.50	4.20
		RQ [21]	68.65	69.54	0.89
ResNet-50	3	GPFQ (Ours)	70.85	76.13	5.28
	4	MSE [1]	73.80	76.10	2.30
		OMSE [3]	73.39	76.01	2.62
		OCS + Clip [35]	69.30	76.10	6.80
		PWLQ [8]	73.70	76.10	2.40
		AdaRound [24]	75.23	76.07	0.84
		S-AdaQuant [14]	75.10	77.20	2.10
		BRECQ [19]	76.29	77.00	0.71
		GPFQ (Ours)	74.21	76.13	1.92
	5	OCS + Clip [35]	73.40	76.10	2.70
		GPFQ (Ours)	75.23	76.13	0.90
	8	IAOI [15]	74.90	76.40	1.50

4. CONCLUSION AND FUTURE WORK

We modified and generalized GPFQ, a post training quantization method that utilizes a greedy path-following mechanism to sequentially quantize the layers of a DNN and we introduced a random subsampling strategy to significantly accelerate the quantization procedure for convolutional layers. We proved that the relative square error of GPFQ admits a linear decay (up to a log factor) with respect to the width of the layer, and we showed that this result holds for fully connected and convolutional layers, under a range of assumptions on the input. We also presented complimentary experiments showing that GPFQ achieves near original accuracy and its performance across various architectures is competitive with state-of-the-art methods. Moreover, we empirically observed that the number of samples used for quantization can be relatively small without adversely affecting generalization accuracy. Finally, we demonstrated our method is compatible with various heuristic modifications that can further improve performance.

Many interesting open problems remain. One exciting avenue is to explore quantization error bounds for multiple layers, and entire networks, which may require more advanced mathematical tools. It also remains to explore variants of GPFQ for recurrent neural networks (RNNs) and other

architectures, including transformers. Incorporating quantization of activations appears compatible with GPFQ, since one can replace the activation $\widetilde{X}_t^{(i-1)}$ in (8) with its quantized counterpart. We leave such an exploration to future work. Another interesting direction is to modify GPFQ to promote desirable properties, e.g. sparsity, in the quantized weights, and to incorporate retraining into the quantization procedure to further boost performance.

ACKNOWLEDGEMENTS

This work was supported in part by National Science Foundation Grant DMS-2012546. The authors thank Eric Lybrand for stimulating discussions on the topics of this paper.

REFERENCES

- [1] R. Banner, Y. Nahshan, E. Hoffer, and D. Soudry. Post-training 4-bit quantization of convolution networks for rapid-deployment. *arXiv preprint arXiv:1810.05723*, 2018.
- [2] Y. Cai, Z. Yao, Z. Dong, A. Gholami, M. W. Mahoney, and K. Keutzer. Zeroq: A novel zero shot quantization framework. In *Proceedings of the IEEE/CVF Conference on Computer Vision and Pattern Recognition*, pages 13169–13178, 2020.
- [3] Y. Choukroun, E. Kravchik, F. Yang, and P. Kisilev. Low-bit quantization of neural networks for efficient inference. In *ICCV Workshops*, pages 3009–3018, 2019.
- [4] M. Courbariaux, Y. Bengio, and J.-P. David. Binaryconnect: Training deep neural networks with binary weights during propagations. In *Advances in neural information processing systems*, pages 3123–3131, 2015.
- [5] J. Deng, W. Dong, R. Socher, L.-J. Li, K. Li, and L. Fei-Fei. Imagenet: A large-scale hierarchical image database. In *2009 IEEE conference on computer vision and pattern recognition*, pages 248–255. Ieee, 2009.
- [6] L. Deng, G. Li, S. Han, L. Shi, and Y. Xie. Model compression and hardware acceleration for neural networks: A comprehensive survey. *Proceedings of the IEEE*, 108(4):485–532, 2020.
- [7] Z. Dong, Z. Yao, A. Gholami, M. W. Mahoney, and K. Keutzer. Hawq: Hessian aware quantization of neural networks with mixed-precision. In *Proceedings of the IEEE/CVF International Conference on Computer Vision*, pages 293–302, 2019.
- [8] J. Fang, A. Shafiee, H. Abdel-Aziz, D. Thorsley, G. Georgiadis, and J. H. Hassoun. Post-training piecewise linear quantization for deep neural networks. In *European Conference on Computer Vision*, pages 69–86. Springer, 2020.
- [9] S. Foucart and H. Rauhut. An invitation to compressive sensing. In *A mathematical introduction to compressive sensing*, pages 1–39. Springer, 2013.
- [10] A. Gholami, S. Kim, Z. Dong, Z. Yao, M. W. Mahoney, and K. Keutzer. A survey of quantization methods for efficient neural network inference. *arXiv preprint arXiv:2103.13630*, 2021.
- [11] Y. Guo. A survey on methods and theories of quantized neural networks. *arXiv preprint arXiv:1808.04752*, 2018.
- [12] S. Han, H. Mao, and W. J. Dally. Deep compression: Compressing deep neural networks with pruning, trained quantization and huffman coding. *arXiv preprint arXiv:1510.00149*, 2015.
- [13] K. He, X. Zhang, S. Ren, and J. Sun. Deep residual learning for image recognition. In *Proceedings of the IEEE conference on computer vision and pattern recognition*, pages 770–778, 2016.
- [14] I. Hubara, Y. Nahshan, Y. Hanani, R. Banner, and D. Soudry. Improving post training neural quantization: Layer-wise calibration and integer programming. *arXiv preprint arXiv:2006.10518*, 2020.
- [15] B. Jacob, S. Kligys, B. Chen, M. Zhu, M. Tang, A. Howard, H. Adam, and D. Kalenichenko. Quantization and training of neural networks for efficient integer-arithmetic-only inference. In

- Proceedings of the IEEE conference on computer vision and pattern recognition*, pages 2704–2713, 2018.
- [16] R. Krishnamoorthi. Quantizing deep convolutional networks for efficient inference: A whitepaper. *arXiv preprint arXiv:1806.08342*, 2018.
- [17] A. Krizhevsky, I. Sutskever, and G. E. Hinton. Imagenet classification with deep convolutional neural networks. *Advances in neural information processing systems*, 25:1097–1105, 2012.
- [18] J. H. Lee, S. Ha, S. Choi, W.-J. Lee, and S. Lee. Quantization for rapid deployment of deep neural networks. *arXiv preprint arXiv:1810.05488*, 2018.
- [19] Y. Li, R. Gong, X. Tan, Y. Yang, P. Hu, Q. Zhang, F. Yu, W. Wang, and S. Gu. Brcq: Pushing the limit of post-training quantization by block reconstruction. *arXiv preprint arXiv:2102.05426*, 2021.
- [20] Y. Liu, W. Zhang, and J. Wang. Zero-shot adversarial quantization. In *Proceedings of the IEEE/CVF Conference on Computer Vision and Pattern Recognition*, pages 1512–1521, 2021.
- [21] C. Louizos, M. Reisser, T. Blankevoort, E. Gavves, and M. Welling. Relaxed quantization for discretized neural networks. In *International Conference on Learning Representations*, 2019.
- [22] E. Lybrand and R. Saab. A greedy algorithm for quantizing neural networks. *Journal of Machine Learning Research*, 22(156):1–38, 2021.
- [23] M. Nagel, M. v. Baalen, T. Blankevoort, and M. Welling. Data-free quantization through weight equalization and bias correction. In *Proceedings of the IEEE/CVF International Conference on Computer Vision*, pages 1325–1334, 2019.
- [24] M. Nagel, R. A. Amjad, M. Van Baalen, C. Louizos, and T. Blankevoort. Up or down? adaptive rounding for post-training quantization. In *International Conference on Machine Learning*, pages 7197–7206. PMLR, 2020.
- [25] J. O. Neill. An overview of neural network compression. *arXiv preprint arXiv:2006.03669*, 2020.
- [26] A. Paszke, S. Gross, F. Massa, A. Lerer, J. Bradbury, G. Chanan, T. Killeen, Z. Lin, N. Gimelshein, L. Antiga, et al. Pytorch: An imperative style, high-performance deep learning library. *Advances in neural information processing systems*, 32:8026–8037, 2019.
- [27] K. Simonyan and A. Zisserman. Very deep convolutional networks for large-scale image recognition. *arXiv preprint arXiv:1409.1556*, 2014.
- [28] C. Szegedy, W. Liu, Y. Jia, P. Sermanet, S. Reed, D. Anguelov, D. Erhan, V. Vanhoucke, and A. Rabinovich. Going deeper with convolutions. In *Proceedings of the IEEE conference on computer vision and pattern recognition*, pages 1–9, 2015.
- [29] M. Tan and Q. Le. Efficientnet: Rethinking model scaling for convolutional neural networks. In *International Conference on Machine Learning*, pages 6105–6114. PMLR, 2019.
- [30] R. Vershynin. *High-dimensional probability: An introduction with applications in data science*, volume 47. Cambridge university press, 2018.
- [31] P. Wang, Q. Chen, X. He, and J. Cheng. Towards accurate post-training network quantization via bit-split and stitching. In *International Conference on Machine Learning*, pages 9847–9856. PMLR, 2020.
- [32] P. Wang, X. He, G. Li, T. Zhao, and J. Cheng. Sparsity-inducing binarized neural networks. In *Proceedings of the AAAI Conference on Artificial Intelligence*, volume 34, pages 12192–12199, 2020.
- [33] S. Xu, H. Li, B. Zhuang, J. Liu, J. Cao, C. Liang, and M. Tan. Generative low-bitwidth data free quantization. In *European Conference on Computer Vision*, pages 1–17. Springer, 2020.
- [34] D. Zhang, J. Yang, D. Ye, and G. Hua. Lq-nets: Learned quantization for highly accurate and compact deep neural networks. In *Proceedings of the European conference on computer vision (ECCV)*, pages 365–382, 2018.
- [35] R. Zhao, Y. Hu, J. Dotzel, C. De Sa, and Z. Zhang. Improving neural network quantization without retraining using outlier channel splitting. In *International conference on machine*

- learning*, pages 7543–7552. PMLR, 2019.
- [36] A. Zhou, A. Yao, Y. Guo, L. Xu, and Y. Chen. Incremental network quantization: Towards lossless cnns with low-precision weights. *arXiv preprint arXiv:1702.03044*, 2017.
 - [37] S. Zhou, Y. Wu, Z. Ni, X. Zhou, H. Wen, and Y. Zou. Dorefa-net: Training low bitwidth convolutional neural networks with low bitwidth gradients. *arXiv preprint arXiv:1606.06160*, 2016.

APPENDIX A. USEFUL LEMMATA

Lemma A.1. *In the context of (7), for any $\widetilde{X}_t^{(i-1)} \neq 0$, we have*

$$q_t = \mathcal{Q}\left(\frac{\langle \widetilde{X}_t^{(i-1)}, u_{t-1} + w_t X_t^{(i-1)} \rangle}{\|\widetilde{X}_t^{(i-1)}\|_2^2}\right).$$

Proof. According to (7), $q_t = \arg \min_{p \in \mathcal{A}} \|u_{t-1} + w_t X_t^{(i-1)} - p \widetilde{X}_t^{(i-1)}\|_2^2$. Expanding the square and removing the terms irrelevant to p , we obtain

$$\begin{aligned} q_t &= \arg \min_{p \in \mathcal{A}} \left(p^2 \|\widetilde{X}_t^{(i-1)}\|_2^2 - 2p \langle \widetilde{X}_t^{(i-1)}, u_{t-1} + w_t X_t^{(i-1)} \rangle \right) \\ &= \arg \min_{p \in \mathcal{A}} \left(p^2 - 2p \cdot \frac{\langle \widetilde{X}_t^{(i-1)}, u_{t-1} + w_t X_t^{(i-1)} \rangle}{\|\widetilde{X}_t^{(i-1)}\|_2^2} \right) \\ &= \arg \min_{p \in \mathcal{A}} \left(p - \frac{\langle \widetilde{X}_t^{(i-1)}, u_{t-1} + w_t X_t^{(i-1)} \rangle}{\|\widetilde{X}_t^{(i-1)}\|_2^2} \right)^2 \\ &= \arg \min_{p \in \mathcal{A}} \left| p - \frac{\langle \widetilde{X}_t^{(i-1)}, u_{t-1} + w_t X_t^{(i-1)} \rangle}{\|\widetilde{X}_t^{(i-1)}\|_2^2} \right| \\ &= \mathcal{Q}\left(\frac{\langle \widetilde{X}_t^{(i-1)}, u_{t-1} + w_t X_t^{(i-1)} \rangle}{\|\widetilde{X}_t^{(i-1)}\|_2^2}\right). \end{aligned}$$

In the last equality, we used the definition of (5). \square

Lemma A.2. *Let $\text{Unif}(B_r)$ denote uniform distribution on the closed ball $B_r \subset \mathbb{R}^m$ with center at the origin and radius $r > 0$. Suppose that random vector $X \in \mathbb{R}^m$ is drawn from $\text{Unif}(B_r)$. Then we have*

$$\mathbb{E}\|X\|_2^2 = \frac{mr^2}{m+2}.$$

Proof. Note that the density function of $\text{Unif}(B_r)$ is given by $f(x) = \frac{1}{\text{vol}(B_r)} \mathbb{1}_{B_r}(x)$ where $\text{vol}(B_r) = r^m \pi^{\frac{m}{2}} / \Gamma(\frac{m}{2} + 1)$ is the volume of B_r . Moreover, by integration in spherical coordinates, one can get

$$\begin{aligned} \mathbb{E}\|X\|_2^2 &= \int_{\mathbb{R}^m} \|x\|_2^2 f(x) dx \\ &= \int_0^\infty \int_{\mathbb{S}^{m-1}} z^{m-1} \|zx\|_2^2 f(zx) d\sigma(x) dz \\ &= \int_0^r \int_{\mathbb{S}^{m-1}} \frac{z^{m+1}}{\text{vol}(B_r)} d\sigma(x) dz \\ &= \frac{\sigma(\mathbb{S}^{m-1})}{\text{vol}(B_r)} \int_0^r z^{m+1} dz \\ &= \frac{mr^2}{m+2}. \end{aligned}$$

Here, $\sigma(\mathbb{S}^{m-1}) = 2\pi^{\frac{m}{2}} / \Gamma(\frac{m}{2})$ is the spherical measure (area) of the unit sphere $\mathbb{S}^{m-1} \subset \mathbb{R}^m$. \square

Orthogonal Projections. Given a closed subspace $S \subseteq \mathbb{R}^m$, we denote the orthogonal projection onto S by P_S . In particular, if $z \in \mathbb{R}^m$ is a vector, then we use P_z and P_{z^\perp} to represent orthogonal projections onto $\text{span}(z)$ and $\text{span}(z)^\perp$ respectively. Hence, for any $x \in \mathbb{R}^m$, we have

$$(20) \quad P_z(x) = \frac{\langle z, x \rangle z}{\|z\|_2^2}, \quad x = P_z(x) + P_{z^\perp}(x), \quad \text{and} \quad \|x\|_2^2 = \|P_z(x)\|_2^2 + \|P_{z^\perp}(x)\|_2^2.$$

Lemma A.3. *Let \mathcal{A} be one of the alphabets defined in (2) and (3) with step size δ , and largest element q_{\max} . Let $\theta_t := \angle(X_t, u_{t-1})$ be the angle between X_t and u_{t-1} . Suppose that $w \in \mathbb{R}^{N_0}$ satisfies $\|w\|_\infty \leq q_{\max}$, and consider the quantization scheme given by (9). Then, for $t = 1, 2, \dots, N_0$, we have*

$$(21) \quad \|u_t\|_2^2 - \|u_{t-1}\|_2^2 \leq \begin{cases} \frac{\delta^2}{4} \|X_t\|_2^2 - \|u_{t-1}\|_2^2 \cos^2 \theta_t & \text{if } \left| w_t + \frac{\|u_{t-1}\|_2}{\|X_t\|_2} \cos \theta_t \right| \leq q_{\max}, \\ 0 & \text{otherwise.} \end{cases}$$

Proof. By applying (20) and (9), we get

$$(22) \quad \begin{aligned} \|P_{X_t}(u_t)\|_2^2 &= \frac{(X_t^\top u_t)^2}{\|X_t\|_2^2} \\ &= \frac{(X_t^\top u_{t-1} + (w_t - q_t)\|X_t\|_2^2)^2}{\|X_t\|_2^4} \|X_t\|_2^2 \\ &= \left(w_t + \frac{X_t^\top u_{t-1}}{\|X_t\|_2^2} - q_t \right)^2 \|X_t\|_2^2 \\ &= \left(w_t + \frac{\|u_{t-1}\|_2}{\|X_t\|_2} \cos \theta_t - q_t \right)^2 \|X_t\|_2^2. \end{aligned}$$

The last equation holds because $X_t^\top u_{t-1} = \|X_t\|_2 \|u_{t-1}\|_2 \cos \theta_t$. Note that

$$\left(w_t + \frac{\|u_{t-1}\|_2}{\|X_t\|_2} \cos \theta_t - q_t \right)^2 - \left(\frac{\|u_{t-1}\|_2}{\|X_t\|_2} \cos \theta_t \right)^2 = \underbrace{\left(w_t + \frac{2\|u_{t-1}\|_2}{\|X_t\|_2} \cos \theta_t - q_t \right)}_{(I)} \underbrace{(w_t - q_t)}_{(II)},$$

$|w_t| \leq q_{\max}$, and $q_t = \mathcal{Q}\left(w_t + \frac{\|u_{t-1}\|_2}{\|X_t\|_2} \cos \theta_t\right)$. If $\left(w_t + \frac{\|u_{t-1}\|_2}{\|X_t\|_2} \cos \theta_t\right) > q_{\max}$, then $q_t = q_{\max}$ and thus $0 \leq q_t - w_t \leq \frac{\|u_{t-1}\|_2}{\|X_t\|_2} \cos \theta_t$. So (I) $\geq w_t + 2(q_t - w_t) - q_t = q_t - w_t \geq 0$ and (II) ≤ 0 . Moreover, if $\left(w_t + \frac{\|u_{t-1}\|_2}{\|X_t\|_2} \cos \theta_t\right) < -q_{\max}$, then $q_t = -q_{\max}$ and $\frac{\|u_{t-1}\|_2}{\|X_t\|_2} \cos \theta_t \leq q_t - w_t \leq 0$. Hence, (I) $\leq w_t + 2(q_t - w_t) - q_t = q_t - w_t \leq 0$ and (II) ≥ 0 . It follows that

$$(23) \quad \left(w_t + \frac{\|u_{t-1}\|_2}{\|X_t\|_2} \cos \theta_t - q_t \right)^2 \leq \left(\frac{\|u_{t-1}\|_2}{\|X_t\|_2} \cos \theta_t \right)^2$$

when $\left| w_t + \frac{\|u_{t-1}\|_2}{\|X_t\|_2} \cos \theta_t \right| > q_{\max}$. Now, assume that $\left| w_t + \frac{\|u_{t-1}\|_2}{\|X_t\|_2} \cos \theta_t \right| \leq q_{\max}$. In this case, since the argument of \mathcal{Q} lies in the active range of \mathcal{A} , we obtain

$$(24) \quad \left(w_t + \frac{\|u_{t-1}\|_2}{\|X_t\|_2} \cos \theta_t - q_t \right)^2 \leq \frac{\delta^2}{4}.$$

Applying (23) and (24) to (22), one can get

$$(25) \quad \|P_{X_t}(u_t)\|_2^2 \leq \begin{cases} \frac{\delta^2}{4} \|X_t\|_2^2 & \text{if } \left| w_t + \frac{\|u_{t-1}\|_2}{\|X_t\|_2} \cos \theta_t \right| \leq q_{\max}, \\ \|u_{t-1}\|_2^2 \cos^2 \theta_t & \text{otherwise.} \end{cases}$$

Further, we have

$$(26) \quad P_{X_t^\perp}(u_t) = P_{X_t^\perp}(u_{t-1} + w_t X_t - q_t X_t) = P_{X_t^\perp}(u_{t-1}).$$

It follows that

$$\begin{aligned}
 \|u_t\|_2^2 - \|u_{t-1}\|_2^2 &= \|P_{X_t}(u_t)\|_2^2 + \|P_{X_t^\perp}(u_t)\|_2^2 - \|u_{t-1}\|_2^2 \\
 &= \|P_{X_t}(u_t)\|_2^2 + \|P_{X_t^\perp}(u_{t-1})\|_2^2 - \|u_{t-1}\|_2^2 && \text{(by (26))} \\
 &= \|P_{X_t}(u_t)\|_2^2 - \|P_{X_t}(u_{t-1})\|_2^2 && \text{(using (20))} \\
 &= \|P_{X_t}(u_t)\|_2^2 - \|u_{t-1}\|_2^2 \cos^2 \theta_t.
 \end{aligned}$$

Substituting $\|P_{X_t}(u_t)\|_2^2$ with its upper bounds in (25), we obtain (21). \square

Lemma A.4. *Let \mathcal{A} be one of the alphabets defined in (2) and (3) with step size $\delta > 0$, and the largest element q_{\max} . Suppose that $w \in \mathbb{R}^{N_0}$ satisfies $\|w\|_\infty \leq q_{\max}$, and consider the quantization scheme given by (9). Additionally, denote the information of the first $t-1$ quantization steps by a σ -algebra \mathcal{F}_{t-1} , and let $\beta, \lambda > 0$, $s^2 \in (0, 1)$. Then the following results hold for $t = 1, 2, \dots, N_0$.*

(1)

$$\mathbb{E}e^{\lambda\|u_t\|_2^2} \leq \max\left\{\mathbb{E}\left(e^{\frac{\lambda\delta^2}{4}\|X_t\|_2^2}e^{\lambda\|u_{t-1}\|_2^2(1-\cos^2\theta_t)}\right), \mathbb{E}e^{\lambda\|u_{t-1}\|_2^2}\right\}$$

(2)

$$\mathbb{E}\left(e^{\lambda\beta\|u_{t-1}\|_2^2(1-\cos^2\theta_t)} \mid \mathcal{F}_{t-1}\right) \leq -\mathbb{E}(\cos^2\theta_t \mid \mathcal{F}_{t-1})(e^{\lambda\beta\|u_{t-1}\|_2^2} - 1) + e^{\lambda\beta\|u_{t-1}\|_2^2}$$

Here, θ_t is the angle between X_t and u_{t-1} .

Proof. (1) In the t -th step, by Lemma A.3, we have

$$\|u_t\|_2^2 - \|u_{t-1}\|_2^2 \leq \begin{cases} \frac{\delta^2}{4}\|X_t\|_2^2 - \|u_{t-1}\|_2^2 \cos^2\theta_t & \text{if } \left|w_t + \frac{\|u_{t-1}\|_2}{\|X_t\|_2} \cos\theta_t\right| \leq q_{\max}, \\ 0 & \text{otherwise,} \end{cases}$$

where $\theta_t = \angle(X_t, u_{t-1})$ is the angle between X_t and u_{t-1} . On the one hand, if $\left|w_t + \frac{\|u_{t-1}\|_2}{\|X_t\|_2} \cos\theta_t\right| \leq q_{\max}$, we obtain

$$(27) \quad \mathbb{E}e^{\lambda\|u_t\|_2^2} = \mathbb{E}\left(e^{\lambda(\|u_t\|_2^2 - \|u_{t-1}\|_2^2)}e^{\lambda\|u_{t-1}\|_2^2}\right) \leq \mathbb{E}\left(e^{\frac{\lambda\delta^2}{4}\|X_t\|_2^2}e^{\lambda\|u_{t-1}\|_2^2(1-\cos^2\theta_t)}\right)$$

On the other hand, if $\left|w_t + \frac{\|u_{t-1}\|_2}{\|X_t\|_2} \cos\theta_t\right| > q_{\max}$, we get

$$(28) \quad \mathbb{E}e^{\lambda\|u_t\|_2^2} = \mathbb{E}\left(e^{\lambda(\|u_t\|_2^2 - \|u_{t-1}\|_2^2)}e^{\lambda\|u_{t-1}\|_2^2}\right) \leq \mathbb{E}e^{\lambda\|u_{t-1}\|_2^2}.$$

Then the inequality in (1) follows from (27) and (28).

(2) Conditioning on \mathcal{F}_{t-1} , the function $f(x) = e^{\lambda\beta x\|u_{t-1}\|_2^2}$ is convex. It follows that

$$\begin{aligned}
 \mathbb{E}\left(e^{\lambda\beta\|u_{t-1}\|_2^2(1-\cos^2\theta_t)} \mid \mathcal{F}_{t-1}\right) &= \mathbb{E}\left(f(\cos^2\theta_t \cdot 0 + (1-\cos^2\theta_t) \cdot 1) \mid \mathcal{F}_{t-1}\right) \\
 &\leq \mathbb{E}\left(\cos^2\theta_t + (1-\cos^2\theta_t)e^{\lambda\beta\|u_{t-1}\|_2^2} \mid \mathcal{F}_{t-1}\right) \\
 &\leq \mathbb{E}(\cos^2\theta_t \mid \mathcal{F}_{t-1}) + (1 - \mathbb{E}(\cos^2\theta_t \mid \mathcal{F}_{t-1}))e^{\lambda\beta\|u_{t-1}\|_2^2} \\
 &= -\mathbb{E}(\cos^2\theta_t \mid \mathcal{F}_{t-1})(e^{\lambda\beta\|u_{t-1}\|_2^2} - 1) + e^{\lambda\beta\|u_{t-1}\|_2^2}.
 \end{aligned}$$

\square

APPENDIX B. PROOF OF THEOREM 2.1

Proof. Let $\alpha > 0$ and $\lambda > 0$. In the t -th step, by Markov's inequality, one can get

$$(29) \quad \mathbb{P}(\|u_t\|_2^2 \geq \alpha) = \mathbb{P}(e^{\lambda\|u_t\|_2^2} \geq e^{\lambda\alpha}) \leq e^{-\lambda\alpha} \mathbb{E}e^{\lambda\|u_t\|_2^2}.$$

According to Lemma A.4,

$$(30) \quad \mathbb{E}e^{\lambda\|u_t\|_2^2} \leq \max\left\{\mathbb{E}\left(e^{\frac{\lambda\delta^2}{4}\|X_t\|_2^2}e^{\lambda\|u_{t-1}\|_2^2(1-\cos^2\theta_t)}\right), \mathbb{E}e^{\lambda\|u_{t-1}\|_2^2}\right\}.$$

Moreover, applying $\|X_t\|_2^2 \leq r^2$ a.s., the law of total expectation, Lemma A.4 (2) with $\beta = 1$, and assumption (10) sequentially, we obtain

$$\begin{aligned}
\mathbb{E}(e^{\frac{\lambda\delta^2}{4}\|X_t\|_2^2} e^{\lambda\|u_{t-1}\|_2^2(1-\cos^2\theta_t)}) &\leq e^{\lambda r^2\delta^2/4} \mathbb{E}e^{\lambda\|u_{t-1}\|_2^2(1-\cos^2\theta_t)} \\
&= e^{\lambda r^2\delta^2/4} \mathbb{E}(\mathbb{E}(e^{\lambda\|u_{t-1}\|_2^2(1-\cos^2\theta_t)} \mid \mathcal{F}_{t-1})) \\
&\leq e^{\lambda r^2\delta^2/4} \mathbb{E}\left(-\mathbb{E}(\cos^2\theta_t \mid \mathcal{F}_{t-1})(e^{\lambda\|u_{t-1}\|_2^2} - 1) + e^{\lambda\|u_{t-1}\|_2^2}\right) \\
&\leq e^{\lambda r^2\delta^2/4} \mathbb{E}(-s^2(e^{\lambda\|u_{t-1}\|_2^2} - 1) + e^{\lambda\|u_{t-1}\|_2^2}) \\
&= (1 - s^2)e^{\lambda r^2\delta^2/4} \mathbb{E}e^{\lambda\|u_{t-1}\|_2^2} + s^2e^{\lambda r^2\delta^2/4}
\end{aligned}$$

Hence, for each t , inequality (30) becomes

$$(31) \quad \mathbb{E}e^{\lambda\|u_t\|_2^2} \leq \max\left\{a\mathbb{E}e^{\lambda\|u_{t-1}\|_2^2} + b, \mathbb{E}e^{\lambda\|u_{t-1}\|_2^2}\right\}.$$

where $a := (1 - s^2)e^{\lambda r^2\delta^2/4}$ and $b := s^2e^{\lambda r^2\delta^2/4}$. Let $t_0 = |\{1 \leq i \leq t : \mathbb{E}e^{\lambda\|u_{i-1}\|_2^2} \leq a\mathbb{E}e^{\lambda\|u_{i-1}\|_2^2} + b\}|$. Then, noting that $u_0 = 0$, the following inequality follows from (31),

$$\begin{aligned}
\mathbb{E}e^{\lambda\|u_t\|_2^2} &\leq a^{t_0} \mathbb{E}e^{\lambda\|u_0\|_2^2} + b(1 + a + \dots + a^{t_0-1}) \\
&= a^{t_0} + \frac{b(1 - a^{t_0})}{1 - a} \\
(32) \quad &\leq 1 + \frac{b}{1 - a}
\end{aligned}$$

where the last inequality holds provided that $a = (1 - s^2)e^{\lambda r^2\delta^2/4} < 1$. Since the result above hold for all $\lambda > 0$ such that $(1 - s^2)e^{\lambda r^2\delta^2/4} < 1$, we can choose $\lambda = \frac{-2\log(1-s^2)}{r^2\delta^2}$. Then we get $a = (1 - s^2)^{1/2}$ and $b = s^2(1 - s^2)^{-1/2}$. It follows from (29) and (32) that

$$\begin{aligned}
\mathbb{P}(\|u_t\|_2^2 \geq \alpha) &\leq e^{-\lambda\alpha} \left(1 + \frac{b}{1 - a}\right) \\
&= \exp\left(\frac{2\alpha \log(1 - s^2)}{r^2\delta^2}\right) \left(1 + \frac{s^2(1 - s^2)^{-1/2}}{1 - (1 - s^2)^{1/2}}\right) \\
&= \exp\left(\frac{2\alpha \log(1 - s^2)}{r^2\delta^2}\right) \left(1 + (1 - s^2)^{-1/2}(1 + (1 - s^2)^{1/2})\right) \\
&= \exp\left(\frac{2\alpha \log(1 - s^2)}{r^2\delta^2}\right) \left(2 + \frac{1}{\sqrt{1 - s^2}}\right) \\
&\leq \exp\left(\frac{-2\alpha s^2}{r^2\delta^2}\right) \left(2 + \frac{1}{\sqrt{1 - s^2}}\right).
\end{aligned}$$

The last inequality can be obtained using the fact $\log(1 + x) \leq x$ for all $x > -1$. Picking $\alpha = \frac{r^2\delta^2 \log N_0}{s^2}$, we get

$$(33) \quad \mathbb{P}\left(\|u_t\|_2^2 \geq \frac{r^2\delta^2}{s^2} \log N_0\right) \leq \frac{1}{N_0^2} \left(2 + \frac{1}{\sqrt{1 - s^2}}\right).$$

From (33) we can first deduce, by setting $t = N_0$ and using the fact $u_{N_0} = Xw - Xq$, that

$$\mathbb{P}\left(\|Xw - Xq\|_2^2 \geq \frac{r^2\delta^2}{s^2} \log N_0\right) \leq \frac{1}{N_0^2} \left(2 + \frac{1}{\sqrt{1 - s^2}}\right).$$

If the activation function φ is L -Lipschitz, then $\|\varphi(Xw) - \varphi(Xq)\|_2 \leq L\|Xw - Xq\|_2$ and thus

$$\mathbb{P}\left(\|\varphi(Xw) - \varphi(Xq)\|_2^2 \geq \frac{r^2\delta^2L^2}{s^2} \log N_0\right) \leq \frac{1}{N_0^2} \left(2 + \frac{1}{\sqrt{1-s^2}}\right).$$

Moreover, applying a union bound over t , yields

$$\mathbb{P}\left(\max_{1 \leq t \leq N_0} \|u_t\|_2^2 \geq \frac{r^2\delta^2}{s^2} \log N_0\right) \leq \frac{1}{N_0} \left(2 + \frac{1}{\sqrt{1-s^2}}\right).$$

□

APPENDIX C. PROOF OF THEOREM 2.2

Due to $\|X_t\|_2^2 = \sum_{i=1}^d \|Y_t^{(i)}\|_2^2$,

$$(34) \quad \mathbb{E}\|X_t\|_2^2 = \sum_{i=1}^d \mathbb{E}\|Y_t^{(i)}\|_2^2 = \sum_{i=1}^d (n\sigma^2 + n(z_t^{(i)})^2) = m\sigma^2 + n \sum_{i=1}^d (z_t^{(i)})^2$$

Additionally, given a unit vector $u = (u^{(1)}, u^{(2)}, \dots, u^{(d)}) \in \mathbb{R}^m$ with $u^{(i)} \in \mathbb{R}^n$, we have $\langle X_t, u \rangle = \sum_{i=1}^d \langle Y_t^{(i)}, u^{(i)} \rangle \sim \mathcal{N}\left(\sum_{i=1}^d z_t^{(i)} u^{(i)\top} \mathbb{1}_n, \sigma^2\right)$. In fact, once we get the lower bound of $\mathbb{E}\frac{\langle X_t, u \rangle^2}{\|X_t\|_2^2}$ as in (10), the quantization error for unbounded data (14) can be derived similarly to the proof of Theorem 2.1, albeit using different techniques. It follows from the Cauchy-Schwarz inequality that

$$(35) \quad \mathbb{E}\frac{\langle X_t, u \rangle^2}{\|X_t\|_2^2} \geq \frac{(\mathbb{E}|\langle X_t, u \rangle|)^2}{\mathbb{E}\|X_t\|_2^2}.$$

$\mathbb{E}\|X_t\|_2^2$ is given by (34) while $\mathbb{E}|\langle X_t, u \rangle|$ can be evaluated by the following results.

Lemma C.1. *Let $Z \sim \mathcal{N}(\mu, \sigma^2)$ be a normally distributed random variable. Then*

$$(36) \quad \mathbb{E}|Z| \geq \sigma \sqrt{\frac{2}{\pi}} \left(1 - \frac{4}{27\pi}\right).$$

Proof. Let $\Psi(x) = \frac{1}{\sqrt{2\pi}} \int_{-\infty}^x e^{-t^2/2} dt$ be the normal cumulative distribution function. Due to $Z \sim \mathcal{N}(\mu, \sigma^2)$, the folded normal distribution $|Z|$ has mean $\mathbb{E}|Z| = \sigma \sqrt{\frac{2}{\pi}} e^{-\mu^2/2\sigma^2} + \mu(1 - 2\Psi(-\frac{\mu}{\sigma}))$. A well-known result [9, 30] that can be used to bound $\Psi(x)$ is

$$(37) \quad \int_x^\infty e^{-t^2/2} dt \leq \min\left(\sqrt{\frac{\pi}{2}}, \frac{1}{x}\right) e^{-x^2/2}, \quad \text{for } x > 0.$$

Additionally, in order to evaluate $\mathbb{E}|Z|$, we will analyze two cases $\mu \geq 0$ and $\mu < 0$.

(I) Suppose $\mu \geq 0$. By (37), we obtain

$$\begin{aligned} \mathbb{E}|Z| &= \sigma \sqrt{\frac{2}{\pi}} e^{-\mu^2/2\sigma^2} + \mu - 2\mu\Psi(-\mu/\sigma) \\ &= \sigma \sqrt{\frac{2}{\pi}} e^{-\mu^2/2\sigma^2} + \mu - \mu \sqrt{\frac{2}{\pi}} \int_{\mu/\sigma}^\infty e^{-t^2/2} dt \\ &\geq \sigma \sqrt{\frac{2}{\pi}} e^{-\mu^2/2\sigma^2} + \mu - \min\left(\mu, \sigma \sqrt{\frac{2}{\pi}}\right) e^{-\mu^2/2\sigma^2}. \end{aligned}$$

If $\mu \geq \sigma \sqrt{\frac{2}{\pi}}$, then one can easily get

$$\mathbb{E}|Z| \geq \mu \geq \sigma \sqrt{\frac{2}{\pi}}.$$

Further, if $0 \leq \mu < \sigma\sqrt{\frac{2}{\pi}}$, then $\mathbb{E}|Z| \geq (\sigma\sqrt{2/\pi} - \mu)e^{-\mu^2/2\sigma^2} + \mu$. Due to $e^x \geq 1 + x$ for all $x \in \mathbb{R}$, one can get

$$\begin{aligned}\mathbb{E}|Z| &\geq (\sigma\sqrt{2/\pi} - \mu)(1 - \mu^2/2\sigma^2) + \mu \\ &= \frac{1}{2\sigma^2}\mu^3 - \frac{1}{\sigma\sqrt{2\pi}}\mu^2 + \sigma\sqrt{\frac{2}{\pi}} \\ &\geq \sigma\sqrt{\frac{2}{\pi}}\left(1 - \frac{4}{27\pi}\right).\end{aligned}$$

In the last inequality, we optimized in $\mu \in (0, \sigma\sqrt{2/\pi})$ and thus chose $\mu = \frac{2}{3} \cdot \sigma\sqrt{\frac{2}{\pi}}$.
(II) Now we assume $\mu < 0$. It follows from (37) that

$$\begin{aligned}\mathbb{E}|Z| &= \sigma\sqrt{\frac{2}{\pi}}e^{-\mu^2/2\sigma^2} + \mu - 2\mu\Psi(-\mu/\sigma) \\ &= \sigma\sqrt{\frac{2}{\pi}}e^{-\mu^2/2\sigma^2} + \mu - 2\mu\left(1 - \frac{1}{\sqrt{2\pi}}\int_{-\mu/\sigma}^{\infty} e^{-t^2/2} dt\right) \\ &\geq \sigma\sqrt{\frac{2}{\pi}}e^{-\mu^2/2\sigma^2} - \mu + \max\left(\mu, -\sigma\sqrt{\frac{2}{\pi}}\right)e^{-\mu^2/2\sigma^2}.\end{aligned}$$

If $\mu \leq -\sigma\sqrt{\frac{2}{\pi}}$, then we have

$$\mathbb{E}|Z| \geq -\mu \geq \sigma\sqrt{\frac{2}{\pi}}.$$

Moreover, when $-\sigma\sqrt{\frac{2}{\pi}} < \mu < 0$, using the fact $e^x \geq 1 + x$ again, we obtain

$$\begin{aligned}\mathbb{E}|Z| &\geq (\sigma\sqrt{2/\pi} + \mu)(1 - \mu^2/2\sigma^2) - \mu \\ &= -\frac{1}{2\sigma^2}\mu^3 - \frac{1}{\sigma\sqrt{2\pi}}\mu^2 + \sigma\sqrt{\frac{2}{\pi}} \\ &\geq \sigma\sqrt{\frac{2}{\pi}}\left(1 - \frac{4}{27\pi}\right).\end{aligned}$$

The last inequality was derived by optimizing in $\mu \in (-\sigma\sqrt{2/\pi}, 0)$ and choosing $\mu = -\frac{2}{3} \cdot \sigma\sqrt{\frac{2}{\pi}}$.

Combining above results, (36) holds. \square

Lemma C.2. *Let clustered data $X = [X_1, X_2, \dots, X_{N_0}] \in \mathbb{R}^{m \times N_0}$ be defined as in (14) and $u \in \mathbb{R}^m$ be a unit vector. Then, for $1 \leq t \leq N_0$, we have*

$$(38) \quad \mathbb{E} \frac{\langle X_t, u \rangle^2}{\|X_t\|_2^2} \geq \frac{5}{9} \cdot \frac{\sigma^2}{m(\sigma^2 + \max_{1 \leq i \leq d} \|z^{(i)}\|_\infty^2)}.$$

Proof. Since $\langle X_t, u \rangle$ is normally distributed with variance σ^2 , (36) implies

$$\mathbb{E}|\langle X_t, u \rangle| \geq \sigma\sqrt{\frac{2}{\pi}}\left(1 - \frac{4}{27\pi}\right).$$

Plugging the inequality above and (34) into (35), we obtain

$$\mathbb{E} \frac{\langle X_t, u \rangle^2}{\|X_t\|_2^2} \geq \frac{(\mathbb{E}|\langle X_t, u \rangle|)^2}{\mathbb{E}\|X_t\|_2^2} \geq \frac{2(1 - \frac{4}{27\pi})^2}{\pi} \cdot \frac{\sigma^2}{m\sigma^2 + n \sum_{i=1}^d (z_t^{(i)})^2} \geq \frac{5}{9} \cdot \frac{\sigma^2}{m\sigma^2 + n \sum_{i=1}^d (z_t^{(i)})^2}.$$

Therefore, (38) holds due to $(z_t^{(i)})^2 \leq \|z^{(i)}\|_\infty^2 \leq \max_{1 \leq i \leq d} \|z^{(i)}\|_\infty^2$ and $m = nd$. \square

Now we are ready to prove Theorem 2.2.

Proof. Let $\alpha > 0$ and $\lambda > 0$. By using exactly the same argument in (29), at the t -th step of (9), we have

$$(39) \quad \mathbb{P}(\|u_t\|_2^2 \geq \alpha) \leq e^{-\lambda\alpha} \mathbb{E} e^{\lambda\|u_t\|_2^2}.$$

Moreover, Lemma A.4 implies

$$(40) \quad \mathbb{E} e^{\lambda\|u_t\|_2^2} \leq \max\left\{\mathbb{E}\left(e^{\frac{\lambda\delta^2}{4}\|X_t\|_2^2} e^{\lambda\|u_{t-1}\|_2^2(1-\cos^2\theta_t)}\right), \mathbb{E} e^{\lambda\|u_{t-1}\|_2^2}\right\}$$

Until now our analysis here has been quite similar to what we did for bounded input data in Theorem 2.1. Nevertheless, unlike Theorem 2.1, we will control the moment generating function of $\|X_t\|_2^2$ because $\|X_t\|_2^2$ is unbounded. Specifically, applying Cauchy-Schwarz inequality and Lemma A.4 (2) with $\beta = 2$, we obtain

$$(41) \quad \begin{aligned} \mathbb{E}\left(e^{\frac{\lambda\delta^2}{4}\|X_t\|_2^2} e^{\lambda\|u_{t-1}\|_2^2(1-\cos^2\theta_t)} \mid \mathcal{F}_{t-1}\right) &\leq \left(\mathbb{E} e^{\frac{\lambda\delta^2}{2}\|X_t\|_2^2}\right)^{\frac{1}{2}} \left(\mathbb{E}\left(e^{2\lambda\|u_{t-1}\|_2^2(1-\cos^2\theta_t)} \mid \mathcal{F}_{t-1}\right)\right)^{\frac{1}{2}} \\ &\leq \left(\mathbb{E} e^{\frac{\lambda\delta^2}{2}\|X_t\|_2^2}\right)^{\frac{1}{2}} \left(-\mathbb{E}(\cos^2\theta_t \mid \mathcal{F}_{t-1})(e^{2\lambda\|u_{t-1}\|_2^2} - 1) + e^{2\lambda\|u_{t-1}\|_2^2}\right)^{\frac{1}{2}} \end{aligned}$$

In the first step, we also used the fact that X_t is independent of \mathcal{F}_{t-1} . By (38), we have

$$\mathbb{E}(\cos^2\theta_t \mid \mathcal{F}_{t-1}) = \mathbb{E}\left(\frac{\langle X_t, u_{t-1} \rangle^2}{\|X_t\|_2^2 \|u_{t-1}\|_2^2} \mid \mathcal{F}_{t-1}\right) \geq \frac{5}{9mK} =: s^2.$$

Plugging the inequality above into (41), we get

$$(42) \quad \begin{aligned} \mathbb{E}\left(e^{\frac{\lambda\delta^2}{4}\|X_t\|_2^2} e^{\lambda\|u_{t-1}\|_2^2(1-\cos^2\theta_t)} \mid \mathcal{F}_{t-1}\right) &\leq \left(\mathbb{E} e^{\frac{\lambda\delta^2}{2}\|X_t\|_2^2}\right)^{\frac{1}{2}} \left(-s^2(e^{2\lambda\|u_{t-1}\|_2^2} - 1) + e^{2\lambda\|u_{t-1}\|_2^2}\right)^{\frac{1}{2}} \\ &= \left(\mathbb{E} e^{\frac{\lambda\delta^2}{2}\|X_t\|_2^2}\right)^{\frac{1}{2}} \left(e^{2\lambda\|u_{t-1}\|_2^2}(1-s^2) + s^2\right)^{\frac{1}{2}} \\ &\leq \left(\mathbb{E} e^{\frac{\lambda\delta^2}{2}\|X_t\|_2^2}\right)^{\frac{1}{2}} \left(e^{\lambda\|u_{t-1}\|_2^2}(1-s^2)^{\frac{1}{2}} + s\right) \\ &\leq \left(\mathbb{E} e^{\frac{\lambda\delta^2}{2}\|X_t\|_2^2}\right)^{\frac{1}{2}} \left(e^{\lambda\|u_{t-1}\|_2^2}\left(1 - \frac{1}{2}s^2\right) + s\right) \end{aligned}$$

where the last two inequalities hold due to $(x^2 + y^2)^{\frac{1}{2}} \leq |x| + |y|$ for all $x, y \in \mathbb{R}$, and $(1-x)^{\frac{1}{2}} \leq 1 - \frac{1}{2}x$ whenever $x \leq 1$.

Now we evaluate $\mathbb{E} e^{\frac{\lambda\delta^2}{2}\|X_t\|_2^2}$ and note that

$$(43) \quad \mathbb{E} e^{\frac{\lambda\delta^2}{2}\|X_t\|_2^2} = \mathbb{E} \exp\left(\frac{\lambda\delta^2}{2} \sum_{i=1}^d \|Y_t^{(i)}\|_2^2\right) = \prod_{i=1}^d \mathbb{E} \exp\left(\frac{\lambda\delta^2}{2} \|Y_t^{(i)}\|_2^2\right).$$

Since $Y_t^{(i)} \sim \mathcal{N}(z_t^{(i)} \mathbf{1}_n, \sigma^2 I_n)$, we have

$$\begin{aligned} \mathbb{E} \exp\left(\frac{\lambda\delta^2}{2} \|Y_t^{(i)}\|_2^2\right) &= \left[\frac{1}{\sigma\sqrt{2\pi}} \int_{\mathbb{R}} \exp\left(-\frac{(x - z_t^{(i)})^2}{2\sigma^2} + \frac{\lambda\delta^2 x^2}{2}\right) dx \right]^n \\ &= \left\{ \frac{1}{\sigma\sqrt{2\pi}} \cdot \exp\left(\frac{\lambda\delta^2 (z_t^{(i)})^2}{2 - 2\lambda\delta^2\sigma^2}\right) \int_{\mathbb{R}} \exp\left[-\frac{1 - \lambda\delta^2\sigma^2}{2\sigma^2} \left(x - \frac{z_t^{(i)}}{1 - \lambda\delta^2\sigma^2}\right)^2\right] dx \right\}^n \\ &= \left[(1 - \lambda\delta^2\sigma^2)^{-\frac{1}{2}} \exp\left(\frac{\lambda\delta^2 (z_t^{(i)})^2}{2 - 2\lambda\delta^2\sigma^2}\right) \right]^n \end{aligned}$$

where the last equality holds if $\lambda\delta^2\sigma^2 < 1$ and we use the integral of the normal density function:

$$\left(\frac{1 - \lambda\delta^2\sigma^2}{2\pi\sigma^2}\right)^{\frac{1}{2}} \int_{\mathbb{R}} \exp\left[-\frac{1 - \lambda\delta^2\sigma^2}{2\sigma^2} \left(x - \frac{z_t^{(i)}}{1 - \lambda\delta^2\sigma^2}\right)^2\right] dx = 1.$$

Notice that $\frac{1}{1-x} \leq 1 + 2x$ for $x \in [0, \frac{1}{2}]$ and $1 + x \leq e^x$ for all $x \in \mathbb{R}$. Now, we suppose $\lambda\delta^2\sigma^2 \leq \frac{1}{2}$ and thus

$$(1 - \lambda\delta^2\sigma^2)^{-\frac{1}{2}} = \left(\frac{1}{1 - \lambda\delta^2\sigma^2} \right)^{\frac{1}{2}} \leq (1 + 2\lambda\delta^2\sigma^2)^{\frac{1}{2}} \leq e^{\lambda\delta^2\sigma^2}.$$

It follows that

$$\begin{aligned} \mathbb{E} \exp\left(\frac{\lambda\delta^2}{2} \|Y_t^{(i)}\|_2^2\right) &\leq \left[\exp\left(\lambda\delta^2\sigma^2 + \frac{\lambda\delta^2(z_t^{(i)})^2}{2 - 2\lambda\delta^2\sigma^2}\right) \right]^n \\ &\leq \left[\exp\left(\lambda\delta^2\sigma^2 + \lambda\delta^2(z_t^{(i)})^2\right) \right]^n \\ &\leq \exp\left(n\lambda\delta^2\sigma^2\left(1 + \frac{\|z^{(i)}\|_\infty^2}{\sigma^2}\right)\right) \\ (44) \quad &\leq \exp(nK\lambda\delta^2\sigma^2) \end{aligned}$$

Substituting (44) into (43), we get

$$(45) \quad \mathbb{E} e^{\frac{\lambda\delta^2}{2} \|X_t\|_2^2} \leq e^{ndK\lambda\delta^2\sigma^2} = e^{mK\lambda\delta^2\sigma^2}.$$

Combining (42) and (45), if $\lambda\delta^2\sigma^2 \leq \frac{1}{2}$, then

$$\begin{aligned} \mathbb{E}(e^{\frac{\lambda\delta^2}{4} \|X_t\|_2^2} e^{\lambda\|u_{t-1}\|_2^2(1-\cos^2\theta_t)}) &= \mathbb{E}\left(\mathbb{E}(e^{\frac{\lambda\delta^2}{4} \|X_t\|_2^2} e^{\lambda\|u_{t-1}\|_2^2(1-\cos^2\theta_t)} \mid \mathcal{F}_{t-1})\right) \\ &\leq \mathbb{E}\left(e^{\frac{1}{2}mK\lambda\delta^2\sigma^2} (e^{\lambda\|u_{t-1}\|_2^2} (1 - \frac{1}{2}s^2) + s)\right) \\ &= e^{\frac{1}{2}mK\lambda\delta^2\sigma^2} (1 - \frac{1}{2}s^2) \mathbb{E} e^{\lambda\|u_{t-1}\|_2^2} + s e^{\frac{1}{2}mK\lambda\delta^2\sigma^2} \\ (46) \quad &=: a \mathbb{E} e^{\lambda\|u_{t-1}\|_2^2} + b \end{aligned}$$

with $a := (1 - s^2/2)e^{\frac{1}{2}mK\lambda\delta^2\sigma^2}$ and $b := s e^{\frac{1}{2}mK\lambda\delta^2\sigma^2}$. Plugging (46) into (40), we have $\mathbb{E} e^{\lambda\|u_t\|_2^2} \leq \max\{a \mathbb{E} e^{\lambda\|u_{t-1}\|_2^2} + b, \mathbb{E} e^{\lambda\|u_{t-1}\|_2^2}\}$. Next, similar to the argument in (32), iterating expectations yields

$$\mathbb{E} e^{\lambda\|u_t\|_2^2} \leq a^{t_0} \mathbb{E}(e^{\lambda\|u_0\|_2^2}) + b(1 + a + \dots + a^{t_0}) = a^{t_0} + \frac{b(1 - a^{t_0})}{1 - a} \leq 1 + \frac{b}{1 - a}$$

where the last inequality holds if $a := (1 - s^2/2)e^{mK\lambda\delta^2\sigma^2/2} < 1$. So we can now choose $\lambda = \frac{-\log(1-s^2/2)}{mK\delta^2\sigma^2}$, which satisfies $\lambda\delta^2\sigma^2 \in [0, 1/2]$ as required from before. Indeed, due to $m, K \geq 1$ and $s^2 = \frac{5}{9Km} \leq \frac{5}{9}$, we have $\lambda\delta^2\sigma^2 = \frac{-\log(1-s^2/2)}{mK} \leq -\log(1 - \frac{5}{18}) < \frac{1}{2}$. Then we get $a = (1 - \frac{1}{2}s^2)^{1/2}$

and $b = s(1 - \frac{1}{2}s^2)^{-1/2}$. It follows from (39) and $s^2 = \frac{5}{9mK}$ that

$$\begin{aligned}
\mathbb{P}(\|u_t\|_2^2 \geq \alpha) &\leq e^{-\lambda\alpha} \left(1 + \frac{b}{1-a}\right) \\
&= \exp\left(\frac{\alpha \log(1 - s^2/2)}{mK\delta^2\sigma^2}\right) \left(1 + \frac{s(1 - \frac{1}{2}s^2)^{-1/2}}{1 - \sqrt{1 - s^2/2}}\right) \\
&\leq \exp\left(\frac{-\alpha s^2}{2mK\delta^2\sigma^2}\right) \left(1 + \frac{s(1 - \frac{1}{2}s^2)^{-1/2} + s}{s^2/2}\right) && \text{(since } \log(1+x) \leq x\text{)} \\
&= \exp\left(\frac{-\alpha s^2}{2mK\delta^2\sigma^2}\right) \left(1 + 2\frac{(1 - \frac{1}{2}s^2)^{-1/2} + 1}{s}\right) \\
&= \exp\left(-\frac{5\alpha}{18m^2K^2\delta^2\sigma^2}\right) \left[1 + 6\sqrt{\frac{mK}{5}} \left(1 - \frac{5}{18mK}\right)^{-1/2} + 6\sqrt{\frac{mK}{5}}\right] \\
&\leq c\sqrt{mK} \exp\left(-\frac{\alpha}{4m^2K^2\delta^2\sigma^2}\right)
\end{aligned}$$

where $c > 0$ is an absolute constant. Pick $\alpha = 4m^2K^2\delta^2\sigma^2 \log(N_0^p)$ to get

$$(47) \quad \mathbb{P}\left(\|u_t\|_2^2 \geq 4pm^2K^2\delta^2\sigma^2 \log N_0\right) \leq c\sqrt{mK}N_0^{-p}.$$

From (47) we can first conclude, by setting $t = N_0$ and using the fact $u_{N_0} = Xw - Xq$, that

$$\mathbb{P}\left(\|Xw - Xq\|_2^2 \geq 4pm^2K^2\delta^2\sigma^2 \log N_0\right) \leq \frac{c\sqrt{mK}}{N_0^p}.$$

If the activation function φ is L -Lipschitz, then $\|\varphi(Xw) - \varphi(Xq)\|_2 \leq L\|Xw - Xq\|_2$ and thus

$$\mathbb{P}\left(\|\varphi(Xw) - \varphi(Xq)\|_2^2 \geq 4pm^2K^2L^2\delta^2\sigma^2 \log N_0\right) \leq \frac{c\sqrt{mK}}{N_0^p}.$$

Moreover, applying a union bound over t , yields

$$\mathbb{P}\left(\max_{1 \leq t \leq N_0} \|u_t\|_2^2 \geq 4pm^2K^2\delta^2\sigma^2 \log N_0\right) \leq \frac{c\sqrt{mK}}{N_0^{p-1}}.$$

□

APPENDIX D. EXPERIMENTS WITH AD-HOC TECHNIQUES

TABLE 3. ImageNet Top-1 accuracy with weight quantization.

Model	Bits	Method	Quant Acc (%)	Ref Acc (%)	Acc Drop (%)	
Alexnet	3	GPFQ (Ours)	53.22	56.52	3.30	
		GPFQ (Ours) [†]	54.77	56.52	1.75	
	4	OMSE[3]	55.52	56.62	1.10	
		GPFQ (Ours)	55.15	56.52	1.37	
		GPFQ (Ours) [†]	55.51	56.52	1.01	
	5	GPFQ (Ours)	55.67	56.52	0.85	
		GPFQ (Ours) [†]	55.94	56.52	0.58	
	8	DoReFa [37]	53.00	55.90	2.90	
VGG-16	3	GPFQ (Ours)	69.67	71.59	1.92	
		GPFQ (Ours) [†]	70.24	71.59	1.35	
	4	MSE [1]	70.50	71.60	1.10	
		OMSE [3]	71.48	73.48	2.00	
		GPFQ (Ours)	70.70	71.59	0.89	
		GPFQ (Ours) [†]	70.90	71.59	0.69	
	5	GPFQ (Ours)	70.96	71.59	0.63	
		GPFQ (Ours) [†]	71.05	71.59	0.54	
	8	Lee et al. [18]	68.05	68.34	0.29	
	ResNet-18	3	GPFQ (Ours)	65.81	69.75	3.94
			GPFQ (Ours) [†]	66.95	69.75	2.80
		4	MSE [1]	67.00	69.70	2.70
OMSE [3]			68.38	69.64	1.26	
S-AdaQuant [14]			69.40	71.97	2.57	
AdaRound [24]			68.71	69.68	0.97	
BRECQ [19]			70.70	71.08	0.38	
GPFQ (Ours)			68.13	69.76	1.63	
5		GPFQ (Ours) [†]	68.51	69.76	1.25	
		RQ [21]	65.10	69.54	4.44	
6		GPFQ (Ours)	69.04	69.75	0.71	
		GPFQ (Ours) [†]	69.18	69.76	0.58	
ResNet-50		3	DFQ [23]	66.30	70.50	4.20
			RQ [21]	68.65	69.54	0.89
		4	GPFQ (Ours)	70.85	76.13	5.28
			GPFQ (Ours) [†]	70.63	76.13	5.50
	MSE [1]		73.80	76.10	2.30	
	OMSE [3]		73.39	76.01	2.62	
	OCS + Clip [35]		69.30	76.10	6.80	
	PWLQ [8]		73.70	76.10	2.40	
	AdaRound [24]		75.23	76.07	0.84	
	S-AdaQuant [14]		75.10	77.20	2.10	
	BRECQ [19]		76.29	77.00	0.71	
	GPFQ (Ours)		74.21	76.13	1.92	
	GPFQ (Ours) [†]	74.35	76.13	1.78		
	5	OCS + Clip [35]	73.40	76.10	2.70	
GPFQ (Ours)		75.23	76.13	0.90		
8	GPFQ (Ours) [†]	75.26	76.13	0.87		
	IAOI [15]	74.90	76.40	1.50		

[†] Unquantizing the last layer and applying bias correction.

DEPARTMENT OF MATHEMATICS, UNIVERSITY OF CALIFORNIA SAN DIEGO
Email address: `jiz003@ucsd.edu`

DEPARTMENT OF MATHEMATICS, UNIVERSITY OF CALIFORNIA SAN DIEGO
Email address: `yiz044@ucsd.edu`

DEPARTMENT OF MATHEMATICS AND HALICIOĞLU DATA SCIENCE INSTITUTE, UNIVERSITY OF CALIFORNIA SAN
DIEGO
Email address: `rsaab@ucsd.edu`